Association Euratom - Risø National Laboratory annual progress report 2001

Bindslev, H.; Singh, B.N

Publication date:
2002

Document Version
Publisher's PDF, also known as Version of record

Risø-R-1345(EN)

Association Euratom - Risø National Laboratory Annual Progress Report 2001

Edited by H. Bindslev and B.N. Singh

Risø National Laboratory
June 2002

Abstract The programme of the Research Unit of the Fusion Association Euratom - Risø National Laboratory covers work in fusion plasma physics and in fusion technology. The fusion plasma physics research focuses on turbulence and transport, and its interaction with the plasma equilibrium and particles. The effort includes both first principles based modelling, and experimental observations of turbulence and of fast ion dynamics by collective Thomson scattering. The activities in technology cover investigations of radiation damage of fusion reactor materials. These activities contribute to the Next Step, the Long-term and the Underlying Fusion Technology programme. A summary is presented of the results obtained in the Research Unit during 2001.

ISBN 87-550-3064-5
ISBN 87-550-3065-3 (Internet)
ISSN 0106-2840; 1396-3449

Foreword

Risø participates in the internationally coordinated activities to develop fusion as a major source of energy. The principle being pursued is the fusion of hydrogen isotopes to form helium. This is the process, which powers the sun. To make the fusion process run at a significant rate the hydrogen gas must be heated to high temperatures where it ionises and turns into a plasma. Furthermore, the plasma must be confined to achieve suitable densities and sustain the high temperature. On the sun gravity provides the confinement. On earth, the line we are pursuing, use a magnetic field for the confinement. While fusion holds the promise of providing a sustainable source of energy, which is environmentally sound, it also presents considerable scientific and engineering challenges. Key issues in the final steps towards realising fusion energy production include:

1. Improving the plasma energy confinement, that is the ratio between the energy of the plasma and the heating power required to sustain the plasma energy. Improving energy confinement implies reducing energy transport out of the plasma, which principally is due to turbulence. So what we really need to do is to understand and control turbulence.
2. Channelling the energy of fast ions, produced in fusion reactions, into heating the bulk plasma without driving turbulence and without premature exit the fast ions from the plasma. This requires understanding and control of the dynamics of the fast ions in interaction with other particles and with waves.
3. Development of materials, which maintain required mechanical properties under high and sustained neutron fluxes. Neutrons, produced in the fusion reactions, are not confined by the magnetic field. They pass through the first wall of the chamber surrounding the plasma, slowing down on impact with atoms in the wall, thereby giving rise to dislocations in the wall material, which affect the properties of the material.

Risø contributes to fusion research in all these areas: 1) codes, modelling turbulence and transport, have been developed and are continually improved, and benchmarked against experiments. Particularly exciting were recent investigations of methods for controlling turbulence with externally applied electrostatic fields, with the numerical results matching closely experimental observations. 2) Central to understanding the dynamics of fast ions is the acquisition of temporally and spatially resolved measurements of the fast ion velocity distributions in the plasma. Risø, in collaboration with MIT (USA) and EURATOM partners, is developing and operating millimetre wave based collective Thomson scattering diagnostics at the TEXTOR and ASDEX upgrade tokamaks in FZ-Jülich and the Max-Planck Institute for plasma physics in Garching (near Munich). 3) In the field of irradiated materials research Risø is investigating the properties of copper alloys relevant to the next step in fusion research, ITER, and of iron alloys, which will be an essential component of a commercial fusion power plant.

Henrik Bindslev
Risø National Laboratory
June 2002

Contents

1. Summary of Research Unit activities

The activities in the Research Unit cover two main areas:

Fusion Plasma Physics, which includes:

- *Theoretical and numerical turbulence studies*. Turbulence and the associated anomalous transport is investigated using first principles based models and solving these by means of numerical codes in full toroidal geometry. These models are continuously being developed and benchmarked against existing codes at other associations. Furthermore, the results of the models adapted to linear geometry were successfully reproduced experimental results in linear devices. Strategies for controlling turbulence in these devices have been developed and tested in collaboration with other associations. The dynamics of bursts of fluctuations leading to profile relaxation have been studied in models for flux-driven interchange mode turbulence, where the back reaction of the turbulence on the equilibrium flows and profiles are accounted for.
- *Experimental turbulence studies.* In collaboration with IPP Garching measurements are being performed on the W7-AS stellarator with a collective scattering diagnostic built at Risø.
- *Fast Ion Collective Thomson Scattering.* Risø has taken the lead in the development of fast ion collective Thomson scattering diagnostics for TEXTOR and ASDEX upgrade (AUG). These projects are carried out in close collaborations with MIT, and with the TEC and AUG teams.

Fusion Technology, which includes:

- Experimental and theoretical investigations of the effects of irradiation on the microstructural evolution and on the physical and mechanical properties of metals and alloys relevant to the Next Step, the Long Term and Underlying Fusion Technology Programme.

The **global indicators** for the Research Unit in 2001 are:

• Professional staff	9.4	man-years
• Support staff	4.7	man-years
• Total expenditure - incl. mobility	2.10	MioEuro
• Total Euratom support	0.54	MioEuro

2. Fusion plasma physics

2.1 Introduction

Fusion plasmas, with steep gradients in plasma equilibrium parameters and with populations of energetic ions far from thermal equilibrium, have considerable free energy. This energy drives turbulence, which in turn acts back on the equilibrium profiles and on the dynamics of the fast ions. The turbulence naturally gives rise to enhanced transport, but also sets up zonal flows, which tear the turbulent structures apart and give rise to edge transport barriers; most likely at the root of the H-mode. This non-linear interplay between turbulence and equilibrium also supports transient events reminiscent of Edge Localized Modes (ELMs).

This set of topics is the focus of our research: With first principles based codes we seek to model the interplay between plasma turbulence, transport and equilibrium. This modelling is tested against experimental data, notably edge probe data, in collaboration with other associations. To contribute to the experimental knowledge of edge to core turbulence and dynamics we operate a Collective Thomson Scattering (CTS) diagnostic for measuring density fluctuations across the plasma in the Wendelstein 7-AS stellarator. To elucidate the physics of fast ions and their interplay with turbulence, waves and transient events, we have engaged in a new activity; the diagnosis of confined fast ions by CTS at the TEXTOR and ASDEX upgrade tokamaks.

Our aim is not only understanding of the dynamics, but also identification of external actuators with which the turbulence and transport can be controlled. First demonstrations of edge turbulence control with arrays of electrostatic probes have been made in a linear device in collaboration with other associations. Selective ejection of core fast ions by sawteeth, which in turn can be manipulated by localized heating and current drive, was found in fast ion CTS data obtained at TEXTOR in collaboration with TEC and MIT.

Our fusion plasma physics research programme provides for fruitful collaborations with other academic groups working in non-linear science. A sign of the strength of these collaborations is that a member of our team heads the Research School of Non-linear Science in Denmark.

The activities outlined here have been carried out under the Plasma Physics and Fluid Dynamics Programme in the Optics and Fluid Dynamics Department in Risø.

2.2 Scrape off layer simulations and comparison with experiment

V. Naulin, A.H. Nielsen, M. Endler, Th. Klinger* and H. Thomsen**
*(*IPP Greifswald, Greifswald, Germany)*
volker.naulin@risoe.dk

Many features of magnetically confined plasmas are crucially determined by their interaction with material boundaries or, in other words, by the physics of the edge and the scrape off layer plasma. In the past, turbulence simulations looked at very simple models to get a grip on the basic behaviour of the fluctuations while, on the other hand, detailed plasma wall interactions were modelled in 2D transport codes that basically eliminate the dynamics of turbulence, using parameterisations to include the effects of turbulence and the associated

transport in the modelling. Many effects like pedestal formation, LH transition and ELM generation cannot, however, be treated in such a manner as they are based on the interplay between fluctuations and profile variations. We have therefore upgraded the TYR drift Alfvén turbulence code to include sheath boundary conditions in limiter geometry for parts of the domain. An extension to incorporate the more complex divertor geometry is on its way. The numerical results will be compared with probe measurements from the Wendelstein 7AS devices and JET. The influence of active probes will be modelled additionally and will be used to assess the possibilities of actively influencing the edge turbulence. Figure 1 shows the flux surface averaged plasma potential developing self-consistently in a 3D turbulence simulation.

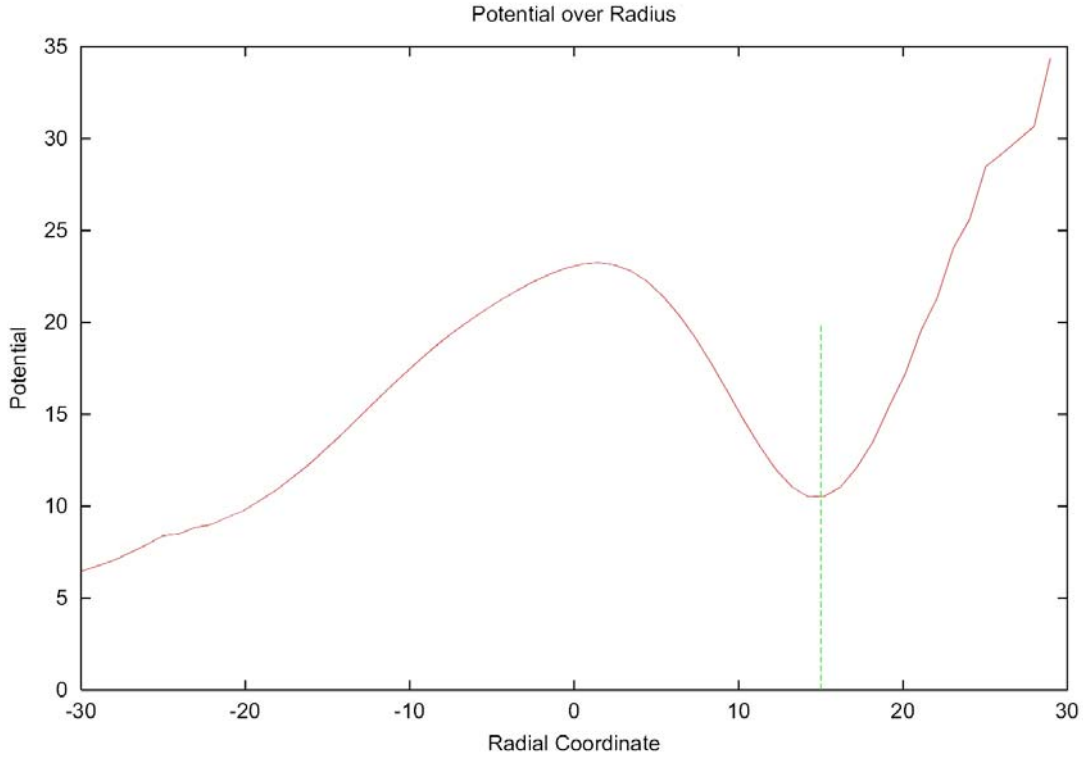

Figure 1. Flux surface averaged plasma potential from a three-dimensional turbulence simulation. Limiter sheath boundary conditions are active outwards from the green line.

2.3 Global dynamics of plasmas

V. Naulin, G. Bonhomme (Laboratoire de Physique des Millieux Ionisés, Université Henri Poincaré Nancy, France), D. Block, F. Greiner*, A. Piel* (*Christian Albrechts Universität Kiel, Germany) and Th. Klinger (IPP Greifswald, Greifswald, Germany)*
volker.naulin@risoe.dk

The complete self-consistent description of even a simple linear plasma is challenging and has as yet not been successfully achieved. Here we try to model the dynamics of a bounded plasma with sources and sinks. The goal is to compare the results with detailed measurements available for these classes of devices like, e.g., the KIWI (Kiel, Germany), the Mirabelle (Nancy, France) and the Vineta (Greifswald, Germany). The results will be used to validate the numerical models used for sheath boundary conditions and for global plasma dynamics.

Furthermore, this model will allow experimental and numerical investigations of wave and turbulence phenomena in parameter regimes relevant to the edge region of existing or upcoming major fusion plasma devices.

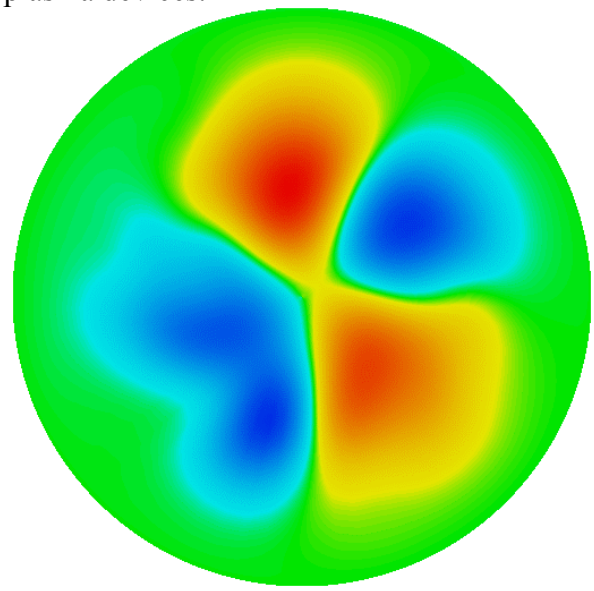

Figure 2. An m = 2 mode with about 3% fluctuation amplitude develops in these 3D simulations of a linear plasma device.

Figure 2 shows the fluctuating part of the density exhibiting an unstable m = 2 mode with a saturated fluctuation amplitude of about 3% of the background density. This numerical result is similar to what is observed in experiments.

2.4 Electromagnetic transport effects

V. Naulin and J. Juul Rasmussen
volker.naulin@risoe.dk

The paradigm for transport barriers is based on the simple argument that sheared flows suppress turbulence and transport via a decorrelation mechanism. Here we present simulation results from the stationary phase of drift-Alfvén turbulence in a sheared 3D geometry. The results show an intrinsic relationship between the shear flows and the magnetic field perturbations, leading to somewhat more complex behaviour, where for larger values of the plasma beta the transport might rise in the presence of shear flows.

The simulations show that the electro-magnetically induced component of the flux – although very small – is localised in just the regions where velocity shear reduces the ExB transport component. This leads to permeability of the transport barrier due to magnetic field line bending by the parallel current component. An ad hoc explanation of this phenomenon can be based on the fact that the ExB shear region is also a transport barrier for the nonlinearly convected parallel current component that thus reaches rather large values just close to the transport barrier. This results in relatively large perturbations of the magnetic field that allow for transport processes parallel to the field lines to somewhat mitigate the effect of the barrier. This is exemplified in Figure 3 that shows that the EM component of the transport is largest where the ExB flux is smallest. Note that in steady state the **total** flux has to be flat as any finite divergence of the flux corresponds to an ongoing profile modification.

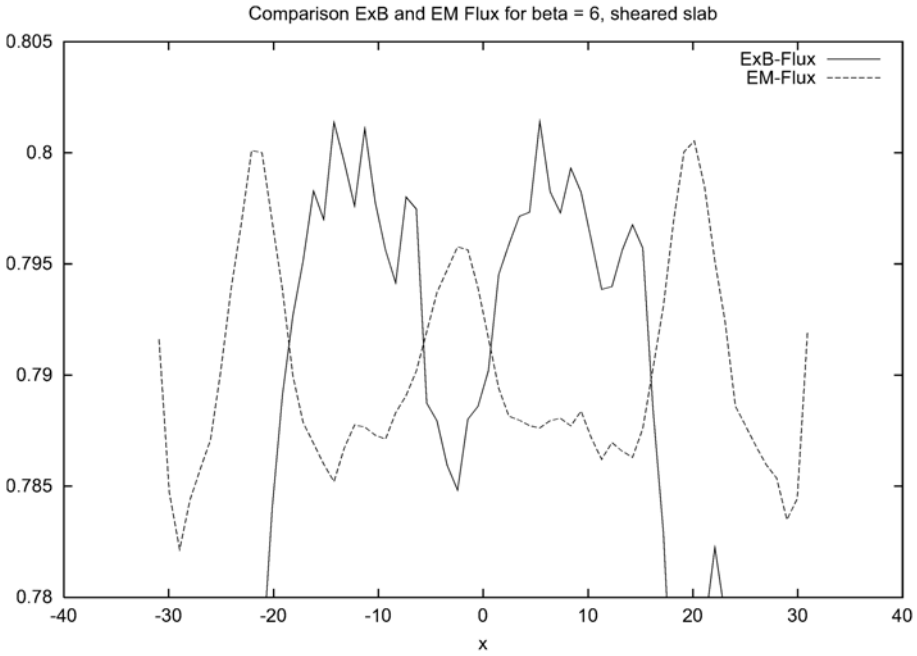

Figure 3. Radial flux surface and time averaged profile of the EXB and the electromagnetic component of the particle flux (note that a constant value of about 0.795 is added to the EM component), showing that the EM component is large where the ExB component is small, namely at the transport barrier.

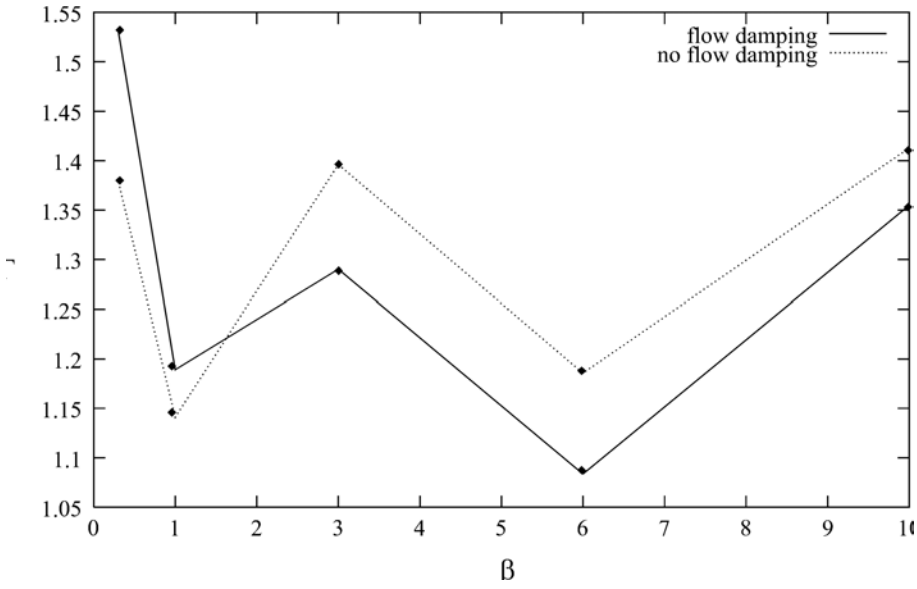

Figure 4. Flux versus normalized plasma beta for runs with and without zonal flow damping. A crossover in the flux scaling can be seen for beta larger then 1.5.

The resulting effect is that when we switch off flow damping in the simulations, the zonal flow level and the transport rise for a plasma beta larger than 1.5. This opposes the simple picture, where an increasing shear flow always leads to a diminished transport. This phenomenon has been depicted in Figure 4 where the flux is shown versus normalized plasma beta for cases with and without zonal flow damping. For a plasma beta larger than 1.5, a crossover in the transport level scaling is visible, marking the onset of the mechanism described above.

2.5 Dispersion of heavy particles in developed drift wave turbulence

R. Basu, V. Naulin and J. Juul Rasmussen
jens.juul.rasmussen@risoe.dk

We have extended the investigation of particle dispersion in drift wave turbulence to account for the dispersion of "heavy" particles. While the dispersion of "plasma ions" is well described by employing the lowest order approximation for their velocity, $\mathbf{v}_{E\times B}$, the E×B velocity (see 2.3), we have to account for inertial effects in the drift velocity of heavier particles. This is incorporated by adding the polarisation velocity, $\mathbf{v}_{pol}$, to the E×B velocity. $\mathbf{v}_{pol}$ depends directly on the mass and the charge of the heavy ion.

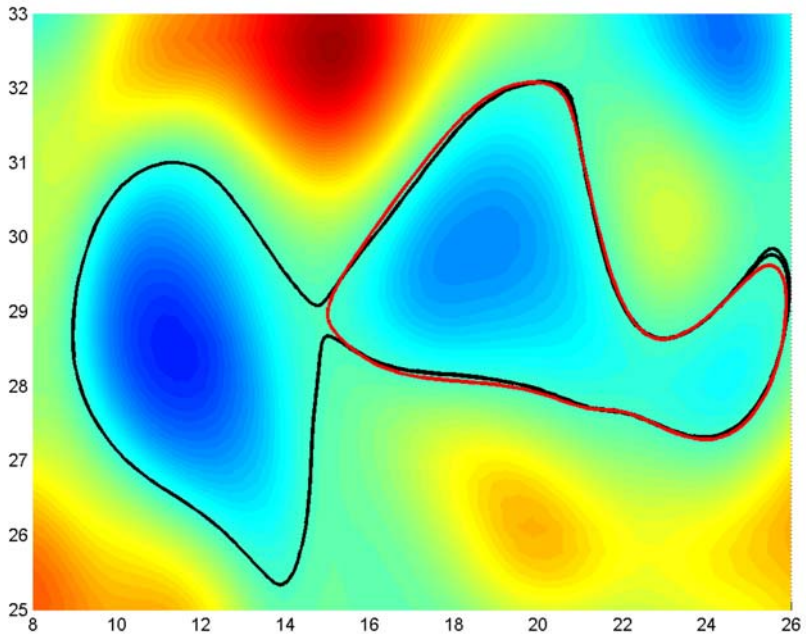

Figure 5. Contour plot of an electrostatic potential. The trajectories of "alpha particles" in a frozen field: red curve: E×B-velocity, only; black curve includes polarisation drift.

The initial results of these investigations are shown in Figure 5 and Figure 6. In Figure 5 we show typical trajectories of a "heavy" ion (parameters like an alpha particle in a hydrogen plasma) in a frozen potential. The red trajectory is the result obtained when using only the E×B velocity, and it is seen that the particle strictly follows the potential contours. The black trajectory is obtained by including $\mathbf{v}_{pol}$. We observe that the trajectory is now deviating from the potential contours and is not necessarily closed, i.e. vortical structures with closed potential contours will not be impermeable to heavy particles. We expect that the dispersion of the heavy particles will be different from the dispersion of the plasma particles. In Figure 6 we have depicted the running diffusion coefficients in the radial as well as in the poloidal direction for "alpha particles" with and without the polarisation drift. We observe an enhanced diffusion.

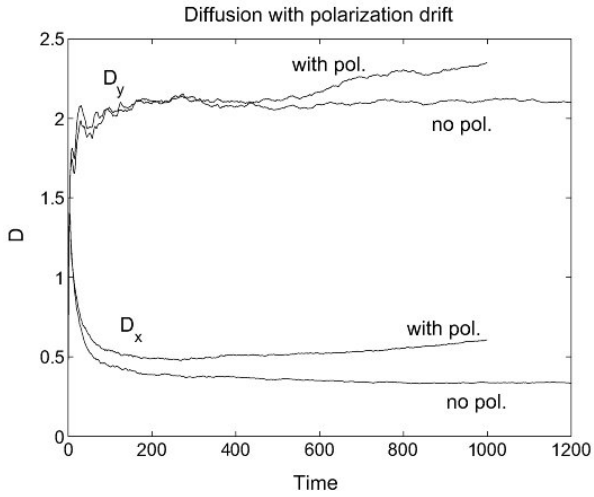

Figure 6. The diffusion coefficients for "alpha particles", with and without the polarisation drift.

2.6 Anomalous diffusion and particle flux

R. Basu, T. Jessen, P.K. Michelsen. V. Naulin, A.H. Nielsen and J. Juul Rasmussen
jens.juul.rasmussen@risoe.dk

The high levels of energy and particle transport across magnetic field lines, known as anomalous transport, are generally agreed to be due to low-frequency turbulence. A good candidate for understanding and explaining this phenomenon from first principles is drift-wave turbulence.

There are two approaches to describe transport in plasma turbulence. One is to look at the convected density, n, leading to an expression $\mathbf{\Gamma} = n\mathbf{v}_{\mathbf{E}\times\mathbf{B}}$ for the density flux, which is usually measured in experiments (here $\mathbf{v}_{\mathbf{E}\times\mathbf{B}}$ is the E×B velocity). The other is to determine a diffusion coefficient from the displacement of test particles. From the outset it is not evident that these two approaches should yield the same result. The flux is degrading the plasma confinement, while the charged particle diffusion reflects the mixing properties of the flow rather than giving information of the direct cross-field transport. A transport of mass is not connected to it, as the centre of mass of the considered test particles stays fixed. We have shown that for drift-wave turbulence the two transport predictions will yield the same result by employing the Langrangian invariance of the potential vorticity. This result is further verified by extensive numerical simulations of drift-wave turbulence based on the Hasegawa-Wakatani model for plasma edge turbulence driven by the resistive instability. That is, we have compared the averaged flux $\langle\mathbf{\Gamma}\rangle$ in the radial direction with the flux obtained from the particle diffusion coefficient via Fick's law.

The trajectories of particles inserted in the turbulent plasma are found by using the first-order drift velocity, $\mathbf{v}_{\mathbf{E}\times\mathbf{B}}$, and the running diffusion coefficient in the radial (x) direction is defined as $D_x(t) = \langle(x - x_0)^2\rangle/2t$, and likewise for the diffusion coefficient in the poloidal (y) direction. We found that the diffusion in the poloidal (y-) direction is significantly larger then the diffusion in the radial (x) direction.[1]

Figure 7 shows the running diffusion coefficient in the radial direction, $D_x(t)$, compared with the diffusion coefficient obtained from the flux by means of Fick's law ($D_{flux} = \langle\mathbf{\Gamma}\rangle/\text{grad } n_0$; for the employed normalizations: $D_{flux} = \langle\mathbf{\Gamma}\rangle$). It is observed that after a transient initial period the two diffusion coefficients are in close agreement. This is observed for a wide range of parameters.

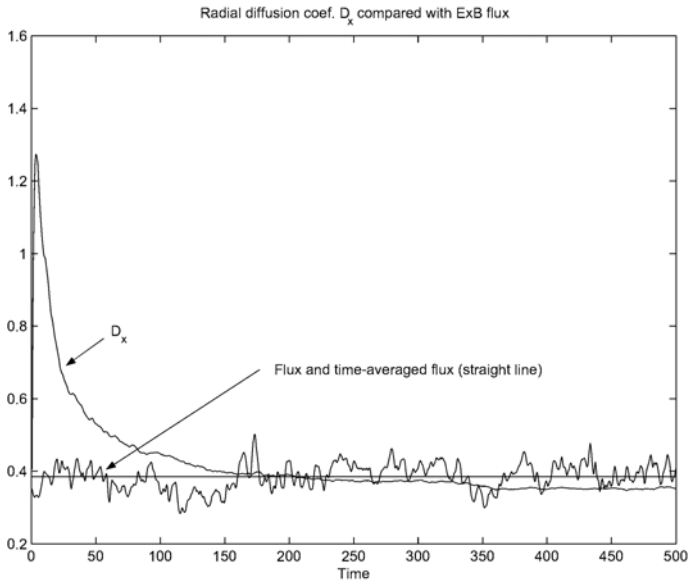

Figure 7. The running diffusion coefficient, D_x, obtained from following the trajectory of 5000 test particles, compared with the turbulent flux.

1. V. Naulin, A.H. Nielsen and J. Juul Rasmussen, *Phys. Plasma* **6**, 4575 (1999).

2.7 Dynamics of transport barriers and ELM-like behaviour in electrostatic turbulence

V. Naulin, J. Nycander (FOA, Stockholm, Sweden) and J. Juul Rasmussen
volker.naulin@risoe.dk

It is generally recognized that self-consistently developing large-scale poloidal - or zonal - flows strongly reduce the radial turbulent transport by "quenching" the turbulence in hot magnetised plasmas. This mechanism may be responsible for the transition to an enhanced confinement, e.g. the H-mode regime first observed in the ASDEX tokamak. The H-mode is often found to be accompanied by bursts in transport related to edge localised modes (ELMs), the so-called ELMy H-mode. If no such intermittent transport behaviour is present, the rising pressure gradients often violently terminate the H-mode plasma by disruptions. Since neither turbulence nor the associated bursty transport can - or should - be avoided, it is essential to understand the interplay between zonal flows (transport barriers) on the one side, and turbulence as well as transport on the other.

We have investigated the evolution and dynamics of transport barriers in the form of zonal flows in a self-consistent model for pressure driven electrostatic turbulence in a plasma in an inhomogeneous magnetic field. This is a simplified model of the outboard side of a toroidal confinement device. It captures the effects of unfavourable curvature in an energy-preserving manner and describes the evolution of profiles as well as fluctuations.

The model is solved numerically on a two-dimensional domain bounded in the radial (x) direction with length L_x and periodic in the poloidal (y) direction with length L_y. The poloidal periodicity length may be interpreted as the recurrence length of a magnetic field line: Assuming an infinite correlation along magnetic field lines for a rational surface characterised by the safety factor q we would have $L_y = 2\pi r/q$.

We have performed numerical simulations for various values of the different parameters of the system: the imposed temperature difference, T_0, the aspect ratio, $a = L_y/L_x$, the size of the system, L_x, and the dissipation coefficients. The behaviour is found to be most sensitive to variations in the aspect ratio, a, which is related to 1/q. When T_0 is sufficiently large to drive the instability, we observe the following general scenarios, depending on aspect ratio as can be seen in Figure 8.

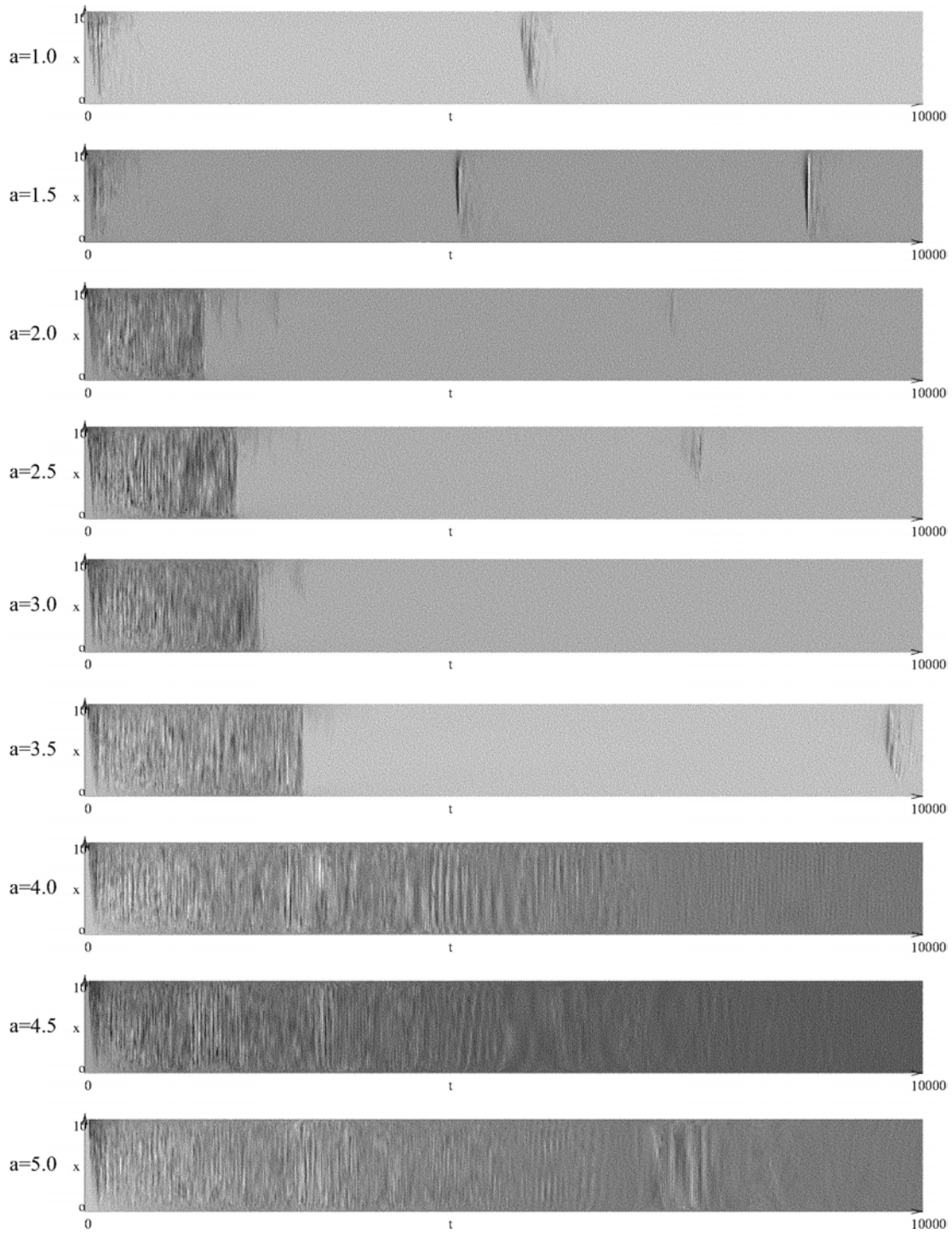

Figure 8. Poloidally averaged flux versus time and radial coordinate for different aspect ratios, a. For an aspect ratio larger than 3.8 no transport suppression is observed.

a) For sufficiently large $a > a_c \sim 3.8$ the system develops into the state of turbulent equipartition (TEP) regardless of the value of T_0, demonstrating profile consistency.[1] This state is accompanied by a radial, turbulent heat flux that is persistent, but intermittent.

b) For smaller a, different behaviour is observed. In an initial phase the turbulence develops and establishes the TEP-profiles with a high flux level. Later on, the flux is interrupted - that is an H-mode-like state with steeper averaged gradients and where lower effective diffusion coefficients develop. For long periods of time the system is very quiescent, as can be seen in Figure 8. However, sporadic flux bursts of high amplitude - analogue to ELMs - are observed to occur at somewhat random intervals. The time scale of the quiescent periods between the bursts is, however, related to the viscous time scale.

The quiet periods are associated with the establishment of a strong poloidal mean flow - the zonal flow - that characterises the transport barrier. This flow, which is strongly sheared and often develops only in a part of the domain, quenches the turbulence and acts as an effective barrier for transport and mixing.

1. V. Naulin, J. Nycander and J. Juul Rasmussen, *Phys. Rev. Lett.* **81**, 4148 (1998).

2.8 Contour dynamics in 2D ideal electronmagnetohydrodynamic flows

S. Senchenko (also at Department of Physics, Technical University of Denmark, Lyngby, Denmark) and V.P. Ruban (Landau Institute for Theoretical Physics, 2 Kosygin str., 117334 Moscow, Russia)
senchen@fysik.dtu.dk

We have considered a special class of vortical flows in plasma that corresponds to the model of the ideal electron magnetohydrodynamics (EMHD). The EMHD model approximately describes the motion of the low-inertial electron component of a plasma on sufficiently short scales (below the ion inertial length). The much heavier ion component may be considered as motionless and is simply providing a static neutralizing background.

The dynamics of vortical structures are investigated by the Hamiltonian method. We follow the evolution of piecewise constant distributions of a conserved quantity related to the frozen-in canonical vorticity. The study includes the case of axisymmetric flows with zero azimuthal velocity component and also the case of flows with the helical symmetry of vortex lines. For an adequately large size of such a patch of the conserved quantity, a local approximation in the dynamics of the patch boundary is suggested. This is based on the possibility of representing the total energy as the sum of area and boundary terms. Only the boundary energy produces deformation of the shape with time. Stationary moving configurations are described.

2.9 Effect of shear flow on drift wave turbulence

S.B. Korsholm, V. Naulin, J. Juul Rasmussen and P.K. Michelsen
soeren.korsholm@risoe.dk

On the path towards future fusion reactors increased attention is given to the importance of turbulence for the efficiency of fusion devices. As a part of these investigations we have looked into the influence of self-generated and externally imposed poloidal shear flows on turbulence levels and turbulent transport. The model used in the numerical investigations is

the three-dimensional drift wave Hasegawa-Wakatani model.[1] The simulations are performed in a slab geometry periodic in y and z (corresponding to the poloidal and toroidal directions, respectively), and in the radial direction we use non-permeable walls, $\phi(x=0)= \phi(x=L_x)=0$ and $n(x=0)=n(x=L_x)=0$, i.e. Dirichlet boundaries in x. ϕ is the electrostatic potential fluctuations, n is the density fluctuations and L_x is the domain length. The simulations are performed using pseudospectral methods.

The energy of the system is defined as $E=\frac{1}{2}\int\left[\left(\nabla_{\perp}\phi\right)^2+n^2\right]d\bar{x}$. In Figure 9 the evolution of the energy of the background flow $E\left(k_y=0,k_{\square}=0\right)$ and the energy of the drift waves $E\left(k_{\square}\neq 0\right)$ is shown, and it is seen that the drift waves are suppressed as the poloidal flow builds up. One may alternatively say that the drift wave turbulence self-organizes into the poloidal shear flow. To illustrate that the sheared flow also reduces the turbulent transport, the maximum shearing rate $\max\left(\frac{\partial v_y}{\partial x}\right)$ and the radial turbulent flux $\Gamma_n=-\int n\frac{\partial\phi}{\partial y}d\bar{x}$ have been plotted in Figure 10. One may see that the turbulent flux has a local minimum when the maximum shearing rate has a local maximum.

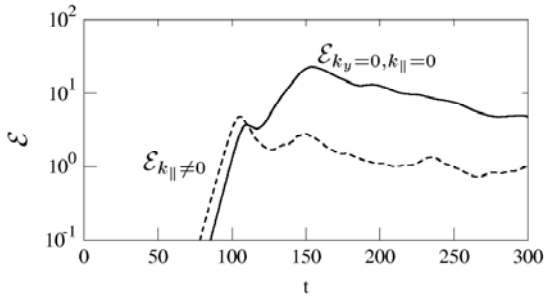

Figure 9. The temporal evolution of the background flow energy (full line) and the drift wave energy (dashed line).

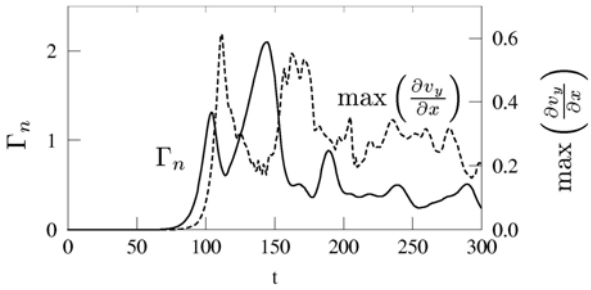

Figure 10. The temporal evolution of the turbulent flux (full line) and the maximum shearing rate (dashed line).

The fluctuations organize to flatten the background profile and this reduces the effective density gradient. Consequently, the drive of the drift wave turbulence is quenched by this backreaction of the density fluctuations. For situations close to adiabaticity $\left(\frac{n}{n_0}\approx\frac{e\phi}{T_e}\right)$ the density flux also arranges for a build-up of a potential profile. This in turn generates shear flow and ultimately suppression of the turbulence.

The shear flow described above is self-generated by the turbulence; however, other effects may lead to a shear flow that also affects the turbulence. We have investigated the effect of an externally imposed shear flow on the turbulence and the flow profiles. We applied a constant shear flow $\overline{v}_S=\overline{v}_S\left(x\right)=\Theta\tanh\left(2\pi(x-L_x/2)\right)\hat{y}$, where Θ is the amplitude of the shear flow.

The external shear flow was applied to the model in such a way that the fluctuations were not allowed to act back on $\overline{v}_S$. In Figure 11a)–c) profiles of the self-generated shear flow $\overline{v}_{E,y}$ as well as the total poloidal shear flow $\overline{v}_{E,y}+\overline{v}_S$ are shown for different values of Θ. Note that for moderate amplitude $\left(\Theta=-1\right)$ the self-generated shear is affected, but maintains its amplitude, whereas for a strong external shear flow the fluctuations are suppressed resulting

in low amplitude of the self-generated shear flow. Finally, in Figure 11d) we present the radial density profile in the case of a strong external shear flow, and it is seen that the shear flow causes a transport barrier to be formed.

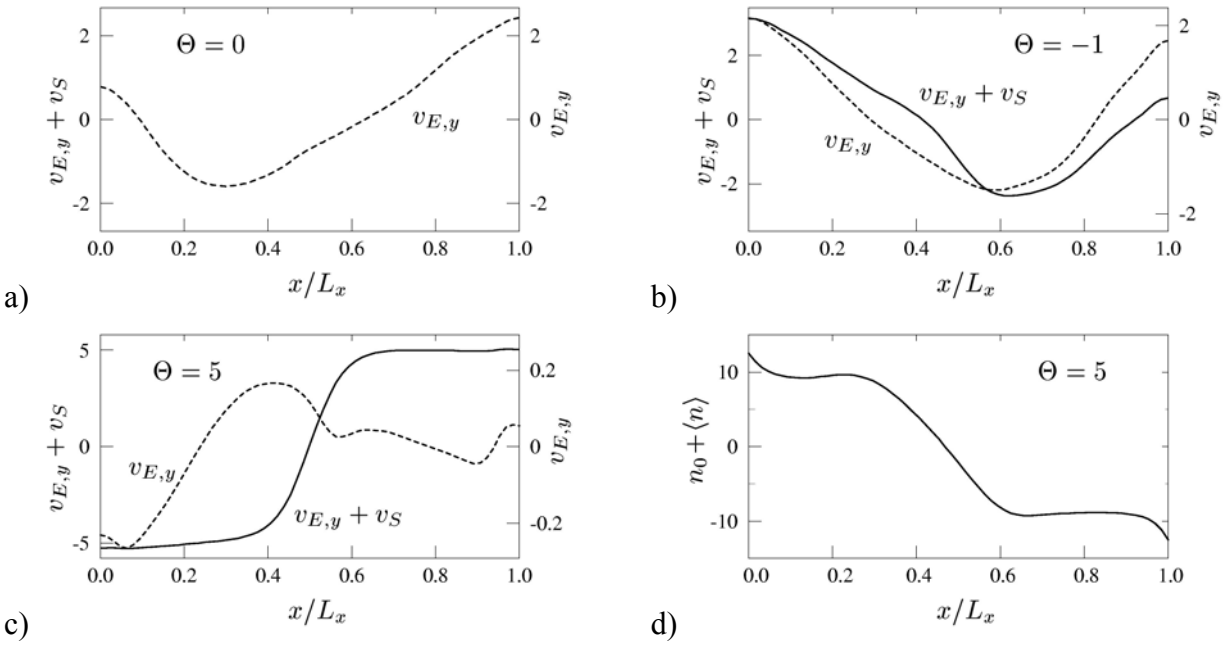

Figure 11. Self-generated shear flow $\overline{v}_{E,y}$ (dashed line) and total shear flow $\overline{v}_{E,y} + \overline{v}_S$ (full line) profiles for a) $(\Theta = 0)$, b) $(\Theta = -1)$ and c) $(\Theta = 5)$; d) the radial density profile for $(\Theta = 5)$. The scale for the full line is to the left.

1. A. Hasegawa and M. Wakatani, *Phys. Rev. Lett.* **50** (1983) 682-686.

2.10 Turbulence in high-density W7-AS divertor plasmas

N.P. Basse, S. Zoletnik (CAT-Science, Budapest, Hungary), M. Saffman (Department of Physics, University of Wisconsin, USA), M. Endler, M. Hirsch* (*Max-Planck-Institut für Plasmaphysik, Garching, Germany), P.K. Michelsen, B.O. Sass, J.C. Thorsen and H.E. Larsen*
nils.basse@risoe.dk

The localised turbulence scattering (LOTUS) density fluctuation diagnostic[1] installed on the Wendelstein 7-AS stellarator was operated routinely during the first six months of 2001. The discharges included partially detached plasmas and record-β shots.

We have here chosen to touch upon measurements in plasmas with extremely high densities and favourable confinement properties; the measurements were obtained using the recently installed divertor modules.[2] This discharge type has provisionally been identified as a high-density H-mode having central densities of up to 4×10^{20} m^{-3}.[3] However, we will here call it improved confinement (IC), while normal confinement is denoted NC.

Two spectrograms are shown in Figure 12, illustrating the differences in density fluctuations between NC (left-hand plot) and IC (right-hand plot). The fluctuations measured in these discharges have a wave number of 20 cm^{-1}, corresponding to spatial scales of 3 mm. The spectra are shown up to frequencies of ± 2 MHz and from 0 to 900 ms; the discharges

were steady state from 400 to 800 ms. It is immediately clear that the fluctuations below ± 1 MHz are larger in IC than NC. The reflectometry system observes the opposite, namely that fluctuations decrease in the NC → IC transition.[4] The difference is likely to be due to the scales observed; fluctuations having much longer wavelengths are observed using reflectometry. However, a reduction in high frequency (> 1.3 MHz) fluctuations is observed using LOTUS. This behaviour could be due to two distinguishable effects: An increase in low-frequency edge fluctuations due to steepening density gradients and a decrease in high-frequency core turbulence. Each effect would be connected to the observed confinement transition.

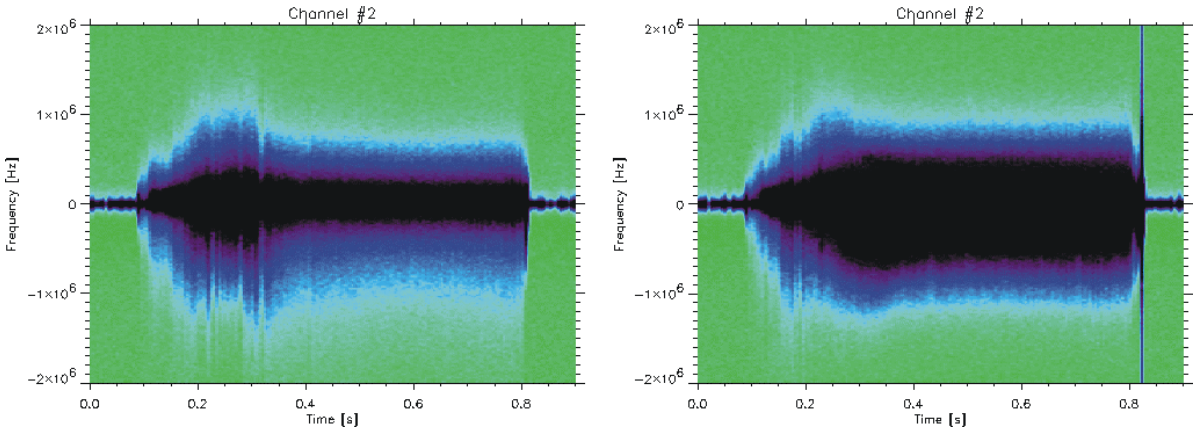

Figure 12. Spectrograms of density fluctuations at 20 cm^{-1} for normal (left) and improved (right) confinement discharges. The colour scale is logarithmic (darker colour means larger amplitude) and identical for both discharges.

1. M. Saffman et al, *Rev. Sci. Instrum.* **72** (2001) 2579.
2. K. McCormick et al., *Plasma Phys. Control. Fusion* **41** (1999) B285.
3. P. Grigull et al., *Plasma Phys. Control. Fusion* **43** (2001) A175.
4. M.Hirsch, private communication (2002).

2.11 Fast ion dynamics measured by collective Thomson scattering

H. Bindslev, P.K. Michelsen, M. Jessen, S. Nimb, J. Thorsen, P. Woskov (MIT, Cambridge, USA), TEC team (FZ-Jülich, Germany; FOM-Rijnhuizen, Netherlands; ERM/KMS, Belgium), ASDEX upgrade team (Max Planck Institute für Plasmaphysik, Garching, Germany)
henrik.bindslev@risoe.dk; www.risoe.dk/euratom/cts

Magnetically confined fusion plasmas contain highly non-thermal populations of fast ions resulting from fusion reactions and plasma heating. With energies in the MeV range, two to three orders of magnitude above the bulk ion and electron energies, the fast ions typically carry one third of the plasma kinetic energy and even more of the free energy. It is essential that these energetic ions remain confined while they slow down and heat the thermal bulk plasma. The free energy associated with the fast ions is, however, also available for mischief. Non-linear wave particle interaction can drive waves and turbulence in the bulk plasma, significantly affecting both bulk and fast ion dynamics. In particular it can lead to catastrophic loss of fast ion confinement. The sawtooth instability, also affected by fast ions, appears to redistribute part of the ion population. If properly tailored, this can be an effective

tool for removing helium ash from the core while leaving the valuable energetic alpha particles in place.

Wave particle interaction is also the basis of ion cyclotron resonance heating (ICRH); one of the main plasma heating schemes relying on the absorption of radio waves. Wave particle interaction depends critically on the phase space distribution of the energetic ions. The effect of waves and turbulence on the ion population manifests itself in the phase space distribution. So both to challenge and guide our understanding of dynamics involving fast ions, and to monitor our attempts at tailoring turbulence and instabilities affecting the ions, we need detailed measurements of the ion phase space distribution.

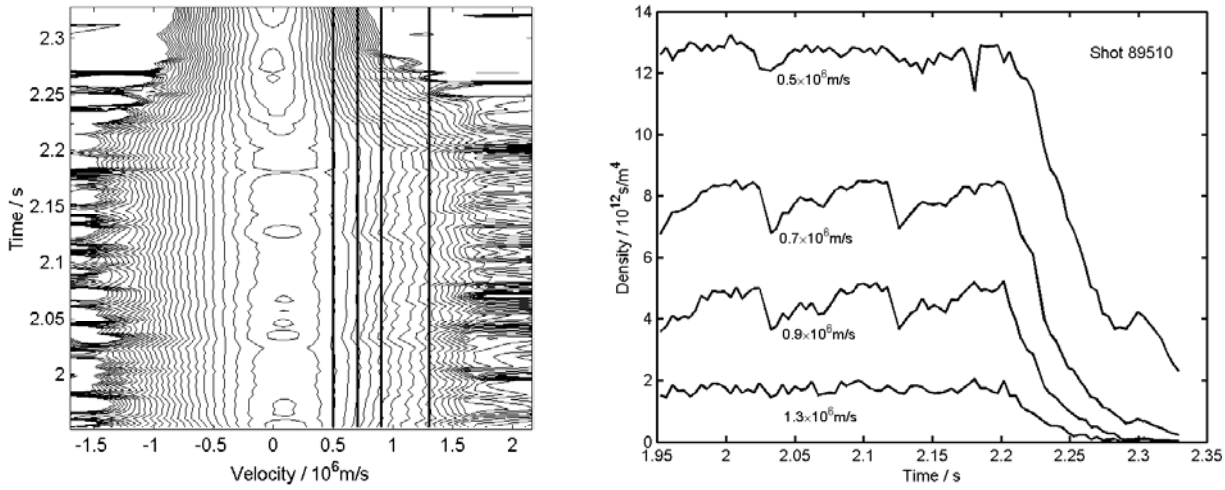

Figure 13. Both plots show the phase space density; number of ions per unit volume and unit velocity. In this shot (89510) the resolved velocity component makes an angle of 65.7° with the static magnetic field. The measurement volume is just to the high field side of the plasma centre, near the electron density inversion radius. Auxiliary heating (ICRH and NBI) is switched off at 2.2 seconds. Left: Contours of the logarithm of the ion phase space density. Right: Time traces of the phase space density for selected velocities.

It has long been realized that collective Thomson scattering (CTS) has a unique capability for diagnosing the ion phase space distribution; that is, it can provide spatially resolved measurements of the velocity distribution. There are other techniques for diagnosing fast ions (charge exchange neutral particle spectroscopy and neutron spectroscopy), but no other diagnostic currently holds the potential for simultaneously resolving the distributions in time, space and velocity. Building on the experience gained with the fast ion CTS diagnostic at JET,[1] the technique had its breakthrough at TEXTOR, where a TEC-MIT team led by H. Bindslev built a proof-of-principle experiment.[2] This experiment demonstrated the feasibility of the measurements[3] and provided a wealth of new data on spatially localised ion velocity distributions at many time points in each plasma shot. These have, among others, permitted the investigation of fast ion dynamics at sawteeth. A sample measurement is shown in Figure 13, where both contours of the logarithm of the phase space density, and time traces for selected velocities have been plotted. The plots show the effects of the switch off of the ion heating at 2.2 s after which the velocity distribution contracts; the energetic ion population decaying in approximately 50 ms. Also evident is the effect of sawteeth. Comparing measurements from like discharges, in which the orientation of the resolved velocity component and the location of the measurement volume were varied independently, both inhomogeneity and anisotropy in the fast ion dynamics at sawteeth were observed.[3]

The CTS effort at TEXTOR continues, now involving also Risø. Additionally, Risø, MIT and the ASDEX upgrade team have started the development of a fast ion CTS at ASDEX upgrade (AUG) tokamak at the Max Planck Institute für Plasmaphysik in Garching

(Munich), Germany. This system will make use of the very substantial investments at AUG in fast ion sources (neutral beam injection and ICRH) and in new megawatt power level gyrotrons to be used as sources of the probing radiation in the CTS system. In addition to permitting fast ion dynamics to be studied in new and more ITER (reactor) relevant conditions, the proposed system for AUG will also provide experience with the use of high-power gyrotrons in a CTS system, as would be required in a fast ion CTS diagnostic for ITER.

1. H. Bindslev, J. A. Hoekzema, J. Egedal, J. A. Fessey, T. P. Hughes and J. S. Machuzak, *Phys. Rev. Lett.* **83**, 3206 (1999).
2. H. Bindslev, L. Porte, A. Hoekzema, J. Machuzak, P. Woskov, and D. van Eester, 26th EPS Conf. Contr. Fusion and Plasma Physics, Maastricht, Netherlands, Vol. 23J, part II, p765, EPS (1999) (http://epsppd.epfl.ch/Maas/web/pdf/p2049.pdf); H. Bindslev, L. Porte, A. Hoekzema, J. Machuzak, P. Woskov, D. van Eester, J. Egedal, J. Fessey and T. Hughes, *Fusion Engineering and Design*, **53**, 105 (2001); H. Bindslev, Journal of Plasma and Fusion Research. 76, 878 (2000); L. Porte, H. Bindslev, F. Hoekzema, J. Machuzak, P. Woskov and D. van Eester, *Rev. Sci. Instrum*. **72**, 1148 (2001); (http://www.risoe.dk/euratom/cts/TEXTOR).
3. H. Bindslev, L. Porte, J. A. Hoekzema, D. van Eester, A. Messiaen, G. van Wassenhove and P. Woskov, Proceedings of the 28th EPS conference on Controlled Fusion and Plasma Physics, Madeira, 18-22 June 2001. http://www.cfn.ist.utl.pt/EPS2001/fin/pdf/P3.077.pdf, (Or.09 & P3.077).

2.12 Publications

2.12.1 International publications

Clercx, H.J.H.; Nielsen, A.H.; Torres, D.J.; Coutsias, E.A., Two-dimensional turbulence in square and circular domains with no-slip walls. *Eur. J. Mech. B* (2001) v. 20 p. 557-576

Bindslev, H.; Porte, L.; Hoekzema, A.; Machuzak, J.; Woskov, P.; van Eester, D.; Egedal, J.; Fessey, J.; Hughes, T. "Fast ion collective Thomson scattering, JET results and TEXTOR plans", Fusion Engineering and Design, 53, 105-111 (2001)

Ditkowski, A.; Dridi, K.H.; Hesthaven, J.S., Convergent Cartesian grid methods for Maxwell's equations in complex geometries. *J. Comput. Phys.* (2001) v. 170 p. 39-80

Donné, A. J. H.; Jaspers, R.; Barth, C. J.; Bindslev, H.; Elzendoorn, B. S. Q.; van Gorkom, J. C.; van der Meiden, H. J.; Oyevaar, T.; van de Pol, M. J.; Udintsev, V. S.; Widdershoven, H. L. M.; Biel, W.; Finken, K. H.; Krämer-Flecken, A.; Kreter, A. et al., " New diagnostics for physics studies on TEXTOR-94", Review of Scientific Instruments, 72, 1046-1053 (2001)

Dridi, K.H.; Hesthaven, J.S.; Ditkowski, A., Staircase-free finite-difference time-domain formulation for general materials in complex geometries. *IEEE Trans. Antennas Propag.* (2001) v. 49 p. 749-756

Germaschewski, K.; Grauer, R.; Bergé, L.; Mezentsev, V.K.; Juul Rasmussen, J., Splittings, coalescence, bunch and snake patterns in the 3D nonlinear Schrödinger equation with anisotropic dispersion. *Physica D* (2001) v. 151 p. 175-198

Karpman, V.I.; Juul Rasmussen, J.; Shagalov, A.G., Dynamics of solitons and quasisolitons of the cubic third-order nonlinear Schrödinger equation. *Phys. Rev. E* (2001) v. 64 p. 026614.1-026614.13

Klinger, T.; Schröder, C.; Block, D.; Greiner, F.; Piel, A.; Bonhomme, G.; Naulin, V., Chaos control and taming of turbulence in plasma devices. *Phys. Plasmas* (2001) v. 8 p. 1961-1968

Korsholm, S.B.; Michelsen, P.K.; Naulin, V.; Juul Rasmussen, J.; Garcia, L.; Carreras, B.A.; Lynch, V.E., Reynolds stress and shear flow generation. *Plasma Phys. Control. Fusion* (2001) v. 43 p. 1379-1397

Porte, L; Bindslev, H.; Hoekzema, F.; Machuzak, J.; Woskov, P.; Van Eester, D. "Implementation of collective Thomson scattering on the TEXTOR tokamak for energetic ion measurements", Review of Scientific Instruments, 72, 1148-1150 (2001)

Ruban, V.P., Slow inviscid flows of a compressible fluid in spatially inhomogeneous systems. *Phys. Rev. E* (2001) v. 64 p. 036305.1-036305.7

Ruban, V.P.; Podolsky, D.I.; Juul Rasmussen, J., Finite time singularities in a class of hydrodynamic models. *Phys. Rev. E* (2001) v. 63 p. 056306.1 - 056306.9

Saffman, M.; Zoletnik, S.; Basse, N.P.; Svendsen, W.; Kocsis, G.; Endler, M., CO_2 laser based two-volume collective scattering instrument for spatially localized turbulence measurements. *Rev. Sci. Instrum.* (2001) v. 72 p. 2579-2592

Schröder, C.; Klinger, T.; Block, D.; Piel, A.; Bonhomme, G.; Naulin, V., Mode selective control of drift wave turbulence. *Phys. Rev. Lett.* (2001) v. 86 p. 5711-5714

Sykes, A.; Akers, R.J.; Appel, L.C.; Arends, E.R.; Carolan, P.G.; Conway, N.J.; Counsell, G.F.; Cunningham, G.; Dnestrovskij, A.; Dnestrovskij, Y.N.; Field, A.R.; Fielding, S.J.; Gryaznevich, M.P.; Korsholm, S.B.; Laird, E.; Martin, R.; Nightingale, M.P.S.; Roach, C.M.; Tournianski, M.R.; Walsh, M.J.; Warrick, C.D.; Wilson, H.R.; You, S., First results from MAST. *Nucl. Fusion* (2001) v. 41 p. 1423-1433

2.12.2 Danish publications

Lynov, J.P.; Singh, B.N (eds.), Association Euratom - Risø National Laboratory annual progress report 2000. Risø-R-1283(EN) (2001) 45 p. www.risoe.dk/rispubl/ofd/ris-r-1283.htm

Lynov, J.P.; Singh, B.N (eds.), Association Euratom - Risø National Laboratory annual progress report 1999. Risø-R-1245(EN) (2001) 48 p. www.risoe.dk/rispubl/ofd/ris-r-1245.htm

2.12.3 Conference lectures

Basse, N.P.; Michelsen, P.K.; Zoletnik, S.; Saffman, M.; Endler, M.; Hirsch, M., Spatial distribution of turbulence in the Wendelstein 7-AS stellarator (invited paper). In: Proceedings. Vol. 4. International conference on phenomena in ionized gases (25. ICPIG), Nagoya (JP), 17-22 Jul 2001. Goto, T. (ed.), (Nagoya University, Nagoya, 2001) p. 335-336

Bindslev, H.; Porte, L.; Hoekzema, J.A.; Woskov, P.; Van Eester, D.; Messiaen, A.; Van Wassenhove, G., Fast ion dynamics in TEXTOR measured by collective Thomson scattering (oral presentation). In: Abstracts of invited and contributed papers. 28. European Physical Society conference on controlled fusion and plasma physics, Funchal (PT), 18-22 Jun 2001. Silva, C.; Varandas, C.; Campbell, D. (eds.), (Instituto Superior Tecnico, Funchal, 2001) p. 144

Porte, L.; Bindslev, H.; Hoekzema, F.; Korsholm, S.B.; Kruyt, O.G.; Prins, R.; Woskov, P., Fast-ion collective Thomson scattering diagnostic on TEXTOR Tokamak (poster). In: Abstracts of invited and contributed papers. 28. European Physical Society conference on controlled fusion and plasma physics, Funchal (PT), 18-22 Jun 2001. Silva, C.; Varandas, C.; Campbell, D. (eds.), (Instituto Superior Tecnico, Funchal, 2001) p. 124

2.12.4 Publications for a broader readership

Juul Rasmussen, J., De forunderlige hvirvler. *Aktuel Naturvidenskab* (2001) (no.2) p. 17-21

2.12.5 Unpublished Danish lectures

Michelsen, P.K., Status for fusionsforskningen. Møde i Kernefysisk Selskab, Ingeniørforeningen i Danmark, København (DK), 19 Mar 2001. Unpublished.

2.12.6 Unpublished international lectures

Akers, R.J.; Appel, L.; Arends,E.R.; Carolan, P.G.; Conway, N.; Counsell, G.; Cunningham, G.; Dnestrovskij, A.; Dnestrovskij, Y.N.; Field, A.R.; Fielding, S.J.; Gryaznevich, M.; Kirk, A.; Korsholm, S.; Laird, E.; Martin, R.; Roach, C.; Sykes, A.; Walsh, M.J.; Warrick, C., Confinement in L and H-mode MAST plasmas (poster). In: Abstracts of invited and contributed papers. 28. European Physical Society conference on controlled fusion and plasma physics, Funchal (PT), 18-22 Jun 2001. Silva, C.; Varandas, C.; Campbell, D. (eds.), (Instituto Superior Tecnico, Funchal, 2001) p. 176

Basse, N.P.; Zoletnik, S.; Saffman, M.; Antar, G.; Michelsen, P.K., Temporal separation of turbulent time series: Measurements and simulations. In: Book of abstracts. 9. European fusion theory conference (EFTC), Elsinore (DK), 17-19 Oct 2001. (Risø National Laboratory, Optics and Fluid Dynamics Department, Roskilde, 2001) p. O-9

Basse, N.P.; Zoletnik, S.; Saffman, M.; Endler, M.; Hirsch, M., Separation of L- and H-mode density fluctuations in dithering Wendelstein 7-AS plasmas (poster). In: Abstracts of invited and contributed papers. 28. European Physical Society conference on controlled fusion and plasma physics, Funchal (PT), 18-22 Jun 2001. Silva, C.; Varandas, C.; Campbell, D. (eds.), (Instituto Superior Tecnico, Funchal, 2001) p. 584

Benilov, E.; Juul Rasmussen, J., Does a sheared current stabilise inversely stratified fluid?. EGS 2001, 26. General assembly, Nice (FR), 25-30 Mar 2001. Unpublished.

Bindslev, H.; Porte, L.; Hoekzema, J. A.; Woskov, P. "Fast ion dynamics measured by Collective Thomson Scattering of mm waves", Invited Lecture at the 10th International Symposium on Laser-Aided Plasma Diagnostics (LAPD-10), Fukuoka, Japan, 24-28 September 2001

Bindslev, H.; Porte, L.; Hoekzema, J. A.; Van Eester, D.; Woskov, P. "Fast ion dynamics measured by Collective Thomson Scattering", Invited Oral at the International conference on Advanced Diagnostics for Magnetic and Inertial Fusion, 3-7 September 2001, Varenna, Italy.

Bindslev, H. "Assessing and Optimising Diagnostic Capabilities of Interdependent Systems", Invited oral at the Wendelstein 7-X data validation workshop Greifswald, 30 July – 1 August 2001

Porte, L.; Bindslev, H.; Hoekzema, F.; Machuzak, J.; Woskov, P. "Fast-Ion Collective Thomson Scattering Diagnostic on TEXTOR Tokamak", poster at the 28th EPS (see above) (P1.110)

Bindslev, H. "Fast ion dynamics measured by collective Thomson scattering", Oral at the 2001 US - European Transport Task Force Meeting, 16-19 May 2001, University of Alaska, Fairbanks.

Bindslev, H. "Fast ion dynamics measured by collective Thomson scattering", Invited Oral at the IEA-DED & IEA-TEXTOR workshop, Jülich, 26-28 March 2001.

Bindslev, H., Fast ion dynamics measured by collective Thomson scattering (invited talk). 43. Annual meeting of the APS Division of Plasma Physics, Long Beach, CA (US), 29 Oct - 2 Nov 2001. Unpublished. Abstract available

Bindslev, H.; Porte, L.; Hoekzema, J.A.; Woskov, P.; Eester, D. Van; Messiaen, A.; Wassenhove, G. Van, Fast ion dynamics in TEXTOR measured by collective Thomson scattering (oral presentation). In: Abstracts of invited and contributed papers. 28. European Physical Society conference on controlled fusion and plasma physics, Funchal (PT), 18-22 Jun 2001. Silva, C.; Varandas, C.; Campbell, D. (eds.), (Instituto Superior Tecnico, Funchal, 2001) p. 144

Juul Rasmussen, J., Generation of large scale flows and transport barriers in plasma turbulence. Workshop on simulation of plasma turbulence and comparison with experiment, Kiel (DE), 7-9 Mar 2001. Unpublished.

Juul Rasmussen, J., Collapse dynamics in nonlinear Schrödinger equations. Seminar at University of Linköping, Department of Physics and Measurement Technology, Linköping (SE), 22 Nov 2001. Unpublished.

Juul Rasmussen, J., Turbulent equipartition (invited talk). Annual meeting og the Swedish Fusion Research Unit, Stockholm (SE), 7-8 Nov 2001. Unpublished.

Juul Rasmussen, J., Fusion research at Risø. Annual meeting og the Swedish Fusion Research Unit, Stockholm (SE), 7-8 Nov 2001. Unpublished.

Juul Rasmussen, J.; Naulin, V.; Nycander, J., Turbulent equipartition and the dynamics of transport barriers in electrostatic turbulence (poster). In: Book of abstracts. 9. European fusion theory conference (EFTC), Elsinore (DK), 17-19 Oct 2001. (Risø National Laboratory, Optics and Fluid Dynamics Department, Roskilde, 2001) ((EN)) p. P1-13

Juul Rasmussen, J.; Naulin, V., Transport of momentum and particles in electrostatic drift wave turbulence. 4. International workshop on nonlinear waves and chaos in space plasmas, Tromsø (NO), 17-22 Jun 2001. Unpublished. Abstract available

Juul Rasmussen, J.; Naulin, V.; Nielsen, A.H., Dynamics of vortex interactins in two-dimensional flows. In: Programme and book of abstracts. International topical conference on plasma physics: New plasma horizons, Faro (PT), 3-7 Sep 2001. (University of Algarve, Faro, 2001) 1 p.

Juul Rasmussen, J.; Naulin, V., Particle diffusion and density flux in anisotropic turbulence dominated by vortical structures. EUROMECH workshop 428: Transport by coherent structures in environmental and geophysical flows, Torino (IT), 26-29 Sep 2001. Unpublished. Abstract available

Korsholm, S.B.; Michelsen, P.K.; Naulin, V.; Juul Rasmussen, J., Reynolds stress and effects of external and self-generated shear flows (poster). In: Book of abstracts. 9. European fusion theory conference (EFTC), Elsinore (DK), 17-19 Oct 2001. (Risø National Laboratory, Optics and Fluid Dynamics Department, Roskilde, 2001) p. P1-6

Korsholm, S.B.; Michelsen, P.K.; Naulin, V.; Juul Rasmussen, J., Analysis of determination of Reynolds stress in drift wave turbulence (poster). In: Abstracts of invited and contributed papers. 28. European Physical Society conference on controlled fusion and

plasma physics, Funchal (PT), 18-22 Jun 2001. Silva, C.; Varandas, C.; Campbell, D. (eds.), (Instituto Superior Tecnico, Funchal, 2001) p. 650

Lehane, I.; Mansfield, M.W.D.; Meyer, H.; Carolan, P.G.; Arends, E.R.; Korsholm, S.B., Impurity radiation amp; Transport in the MAST Tokamak (poster). 43. Annual meeting of the APS Division of Plasma Physics, Long Beach, CA (US), 29 Oct - 2 Nov 2001. Unpublished. Abstract available

Naulin, V., Taming driftwave turbulence: Numerical simulations and experiment. 2001 US - European Transport Task Force meeting, Fairbanks, AK (US), 16-19 May 2001. Unpublished.

Naulin, V., Stabilization of Rayleigh Taylor types of instability by shearing. Seminar on dynamics of complex systems, University of Alaska, Fairbanks, AK (US), 21-23 May 2001. Unpublished.

Naulin, V., Turbulent transport: From fluxes to diffusion coefficients. Workshop on simulation of plasma turbulence and comparison with experiment, Kiel (DE), 7-9 Mar 2001. Unpublished.

Naulin, V., Driving forces and stabilizing agents in turbulence and their signatures. Workshop on simulation of plasma turbulence and comparison with experiment, Kiel (DE), 7-9 Mar 2001. Unpublished.

Naulin, V., Flows and transport in 3D drift Alfven turbulence. Theorie Seminar at Max Planck Institut für Plasmaphysik, Zinnowitz (DE), 19-23 Nov 2001. Unpublished.

Naulin, V., Flows and transport in 3D drift Alfven turbulence. Seminar at IPP Greifswald, Greifswald (DE), 11 Oct 2001. Unpublished.

Naulin, V.; Basu, R.; Jessen, T.; Michelsen, P.K.; Nielsen, A.H.; Juul Rasmussen, J., Particle diffusion and density flux in strong drift-wave turbulence containing vortical structures (poster). In: Book of abstracts. 9. European fusion theory conference (EFTC), Elsinore (DK), 17-19 Oct 2001. (Risø National Laboratory, Optics and Fluid Dynamics Department, Roskilde, 2001) p. P1-11

Naulin, V.; Korsholm, S.B.; Michelsen, P.K.; Juul Rasmussen, J., Flows and transport in 3D drift Alfvén turbulence (invited talk). In: Book of abstracts. 9. European fusion theory conference (EFTC), Elsinore (DK), 17-19 Oct 2001. (Risø National Laboratory, Optics and Fluid Dynamics Department, Roskilde, 2001) p. I-4

Naulin, V.; Schröder, C.; Klinger, T.; Blick, D.; Piel, A.; Bonhomme, G.; Korsholm, S.B., Taming driftwave turbulence: Numerical simulations and experiment (poster). In: Abstracts of invited and contributed papers. 28. European Physical Society conference on controlled fusion and plasma physics, Funchal (PT), 18-22 Jun 2001. Silva, C.; Varandas, C.; Campbell, D. (eds.), (Instituto Superior Tecnico, Funchal, 2001) p. 519

Nielsen, A.H.; Clercx, H.J.H.; Coutsias, E.A., Vortex evolution in forced 2D bounded flow. EGS 2001, 26. General assembly, Nice (FR), 25-30 Mar 2001. Unpublished. Abstract available

Nielsen, A.H.; Clercx, H.J.H.; Coutsias, E.A., A dipole interacting with a curved no-slip wall. New trands in no-slip vortex flows programme workshop, Eindhoven (NL), 17-18 Sep 2001. Unpublished.

Senchenko, S., Stability of weak turbulence Kolmogorov spectra. Nonlinear science festival 3, Lyngby (DK), 12-15 Jun 2001. Unpublished. Abstract available

Senchenko, S., Stability of weak turbulence Kolmogorov spectra. In: Europhysics conference abstracts, vol. 25G. International conference on waves and wave turbulence, Nyborg (DK), 12-15 Aug 2001. (European Physical Society, Paris, 2001) p. 21

3. Fusion technology

3.1 Introduction

The work reported in this section has been carried out in the Materials Research Department. The overall objective of the research activities in this area is to determine the impact of neutron irradiation on physical and mechanical properties of metals and alloys, so that appropriate materials can be chosen for their application in an irradiation environment (e.g. in a fusion reactor). Various experimental techniques are employed to study different aspects of the microstructural evolution during irradiation and the resulting consequences on the post-irradiation physical and mechanical properties of metals and alloys. Computer simulations are carried out to understand the evolution of surviving defects and their clusters in collision cascades. The kinetics of defect accumulation during irradiation and the influence of irradiation-induced defects and their clusters on the deformation behaviour of irradiated metals and alloys are studied theoretically. In the following, the main results of these activities are highlighted.

3.2 Next step technology

3.2.1 **Analysis of stress relaxation during creep-fatigue interaction experiments**[1]

B.N. Singh, J.F. Stubbins (*University of Illinois, Urbana-Champaign, USA) and P. Toft*

The examination of hold time effects in creep-fatigue testing continued during 2001. These tests were conducted so that the hold period was applied while the strain on the specimen was held constant at the maximum point in both tension and in compression. The hold period results in a relaxation of the stress or load on the specimen, due to the creep process. The loading cycle itself provides the fatigue deformation. The stress relaxation during the hold period is an indication of the amount of time-dependent deformation (i.e. creep) that the specimen can undergo to accommodate the strain level. Tests were performed at 22 or 250°C for a dispersion strengthened copper alloy, CuAl25, and a precipitation strengthened copper alloy, CuCrZr. These materials were also examined in the unirradiated and the irradiated conditions to determine the influence of exposure to a neutron environment on mechanical properties.

Examples of the response of the CuAl25 material to fatigue with hold-time loading conditions is shown in Figure 1, where the cycles are shown as a function of test time. In the examples, the specimen is loaded in tension to the maximum strain point and held there for a fixed period. The cycle is then reversed and the specimen is loaded in compression to the minimum strain point and held there for a fixed period. In Figure 1a, the tension and compression hold periods are 10 seconds each, and 100 seconds each in Figure 1b. The curves indicate the total stress on the specimen and how the stress relaxes during the hold periods as a function of time.

[1] Task GB8 – V63 (BL 12.2) and TWO-T507-5

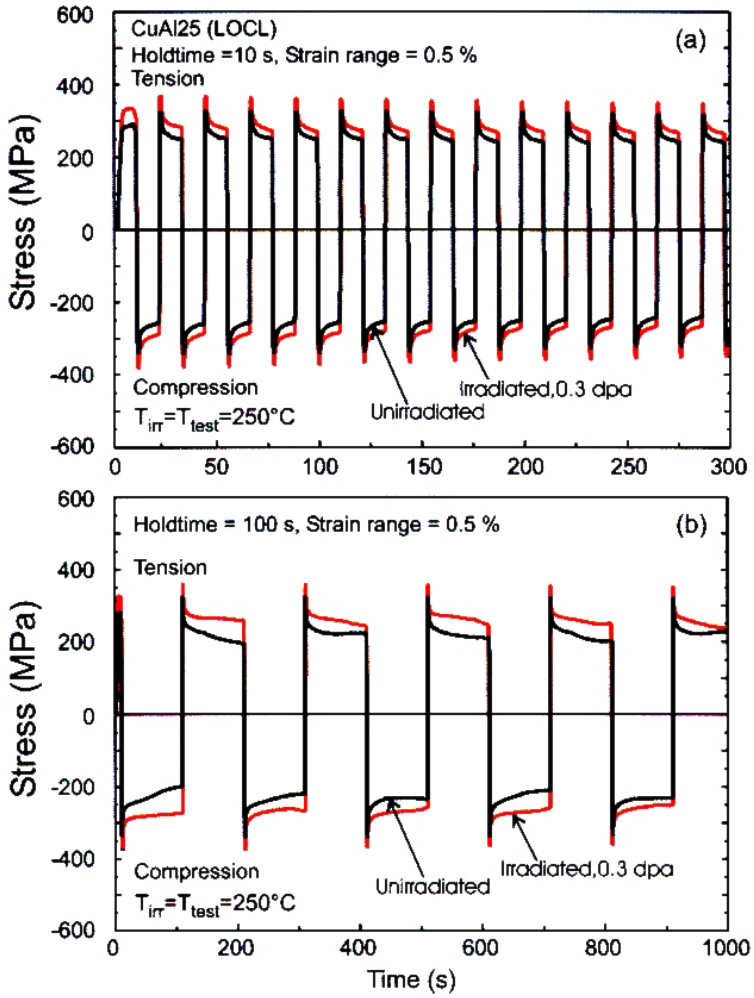

Figure 1. Examples of stress relaxation in unirradiated and irradiated CuAl25 during creep-fatigue tests at 250°C for a strain range value of 0.5% and tested with a holdtime of (a) 10s and (b) 100 s.

Figure 1 shows a comparison of load relaxation for specimens that are unirradiated and specimens that were irradiated to 0.3 dpa (displacements per atom). The test temperature is the same as the irradiation temperature. The maximum tensile and compressive loads are different for the irradiated and unirradiated materials due to the differences in strength with and without irradiation. Nevertheless, significant amounts of stress relaxation take place in all cases.

A direct comparison of the stress relaxation is made in Figures 2 and 3 where the various levels of stress relaxation are shown. The stress drop from the maximum load is plotted as a function of relaxation time for one hold time period in tension. In Figure 2, the stress relaxation values are shown for three different maximum strain levels for two test temperatures. Data for a fourth strain level are also shown from tests conducted at 250°C. It can be seen that the level of relaxation is higher for the higher temperature tests, as would be expected from the increase in creep rate with temperature. It can also be seen that the amount of stress relaxation increases uniformly with increasing level of strain on the specimen. This is the case for both test temperatures. The figure also shows that the magnitude of the stress relaxation is substantial, even for the room temperature tests.

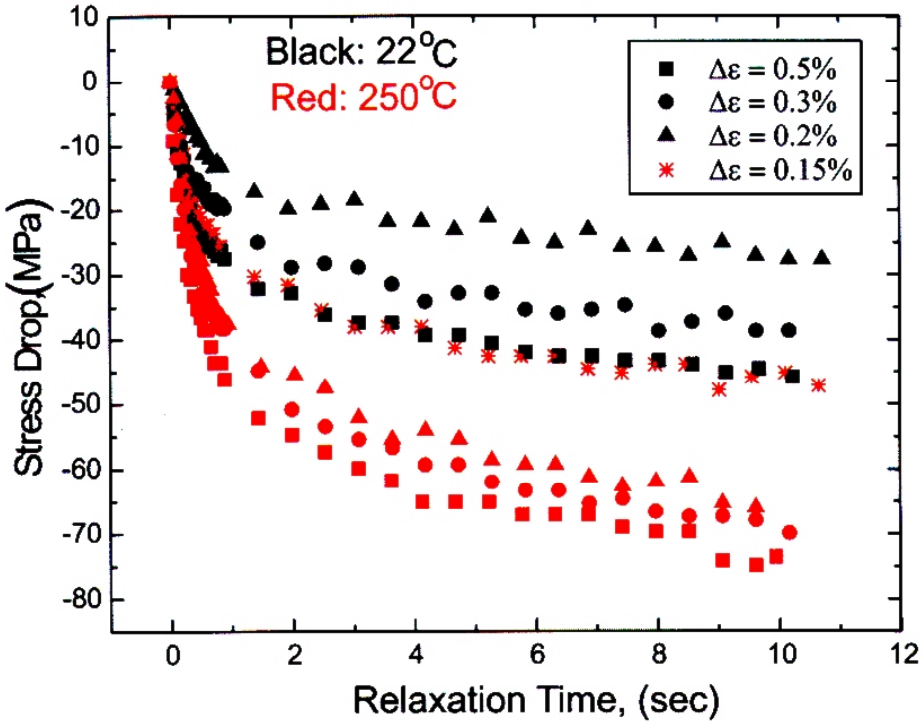

Figure 2. Stress relaxation as a function of time during holdtime of 10 seconds in creep-fatigue tests on CuAl25 at 22 and 250°C for different strain range values (i.e. at different stress levels). Note that the higher the stress level during the holdtime the larger is the stress relaxation.

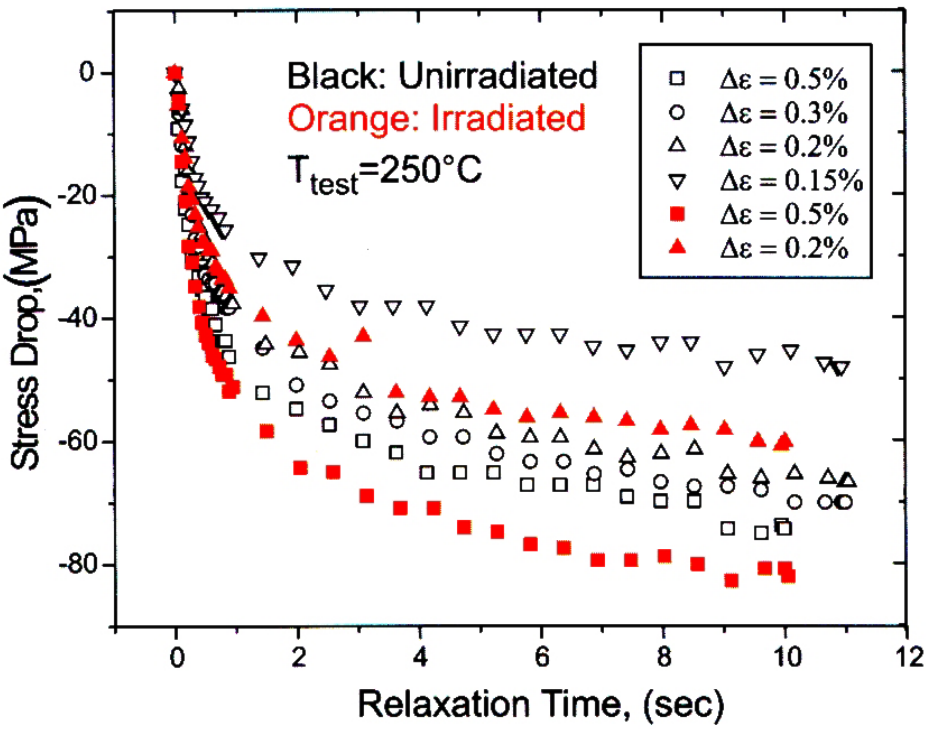

Figure 3. Comparision of stress-relaxation in the unirradiated and irradiated (at 250°C to 0.3 dpa) CuAl25 specimens tested at 250°C with different strain range values. Note that the stress relaxation is larger in the irradiated than that in the unirradiated specimens.

The effect of irradiation on the stress relaxation behaviour is shown in Figure 3 for tests conducted at 250°C. The results for the unirradiated material are the same as shown in Figure 2, where the temperature effect is indicated. The results for the higher strain range are also the same results as shown in Figure 1a where the time dependence and the absolute level of the applied stress can be seen. The irradiated material shows a similar level of stress relaxation for the lower of the two strain ranges. At the high strain range, the level of relaxation is higher for the irradiated material. By comparison with Figure 1, it is seen that the irradiated material has a noticeably higher strength than the unirradiated material. This accounts for the differences in the stress relaxation.

This work is continuing so that these processes can be studied in a wider variety of loading conditions and temperatures. This work will also provide the foundation for a physical understanding of the mechanisms involved in the creep-fatigue interaction processes. To do so, it is necessary not only to perform the proper tests, but the microstructure of the material and the morphology of the fracture surfaces must also be examined to determine the microstructural processes which control the material deformation response.

3.2.2 Impact of creep-fatigue interaction on performance and lifetime of CuCrZr alloy[2]

B.N. Singh, J.F. Stubbins (*University of Illinois, Urbana-Champaign, USA) and P. Toft*

Both the first wall and divertor components of ITER will be exposed to an intense flux of fusion (14 MeV) neutrons and will experience thermomechanical cyclic loading as a result of the cyclic nature of plasma burn operations of the system. Consequently, the materials used in these components will have to endure not only cyclic loading but also stress relaxation (i.e. creep) during the "plasma-on" and "plasma-off" periods. In order to evaluate the impact of this interaction (i.e. creep-fatigue), investigations were initiated to determine the lifetime of CuAl-25 and CuCrZr alloys under the conditions of creep-fatigue interaction. The main results on the CuAl-25 alloy and only a few results on CuCrZr were reported last year. In the following, the rest of the results on CuCrZr alloy are summarised.

Creep-fatigue interaction studies were performed on 39 mm long fatigue specimens with a gauge length and diameter of 7 and 3 mm, respectively. Fatigue specimens were manufactured from the stock of CuCrZr alloy supplied by Outokumpu OY (Finland). The CuCrZr alloy was used in the prime aged condition. A number CuCrZr alloy specimens were tested at 22^{o}C with a strain range of 0.5% also in the prime aged and annealed (600^{o}C for 1 h) condition. Creep-fatigue interaction tests were carried out on unirradiated specimens at 22 and 250^{o}C. Tests of 250^{o}C were carried out in vacuum (<10^{-4} torr).

The creep-fatigue interaction condition was simulated by applying a certain holdtime on both tension and compression sides of the cyclic loading with a frequency of 0.5 Hz for zero holdtime. Tests were carried out in the fully reversed and strain controlled mode. Holdtimes of 2, 5, 10, 100 and 1000 seconds were used. For a given holdtime, the number of cycles to failure was determined at different strain amplitudes. Figure 4 shows examples of cyclic loading at a fixed strain range value of 0.2% both in tension and compression carried out at 22^{o}C for holdtimes of (a) 10 seconds and (b) 100 seconds. It can be seen that during the holdtime the stress (reached at the strain range value of 0.2%) relaxes very rapidly at the beginning of the holdtime and then slows down as a function of time. The process is repeated in each cycle. The nature and the magnitude of stress relaxation in the tension and compression side of the cycles are very similar.

[2] Task GB8-V63 (BL 12.2) and TWO-T507-5

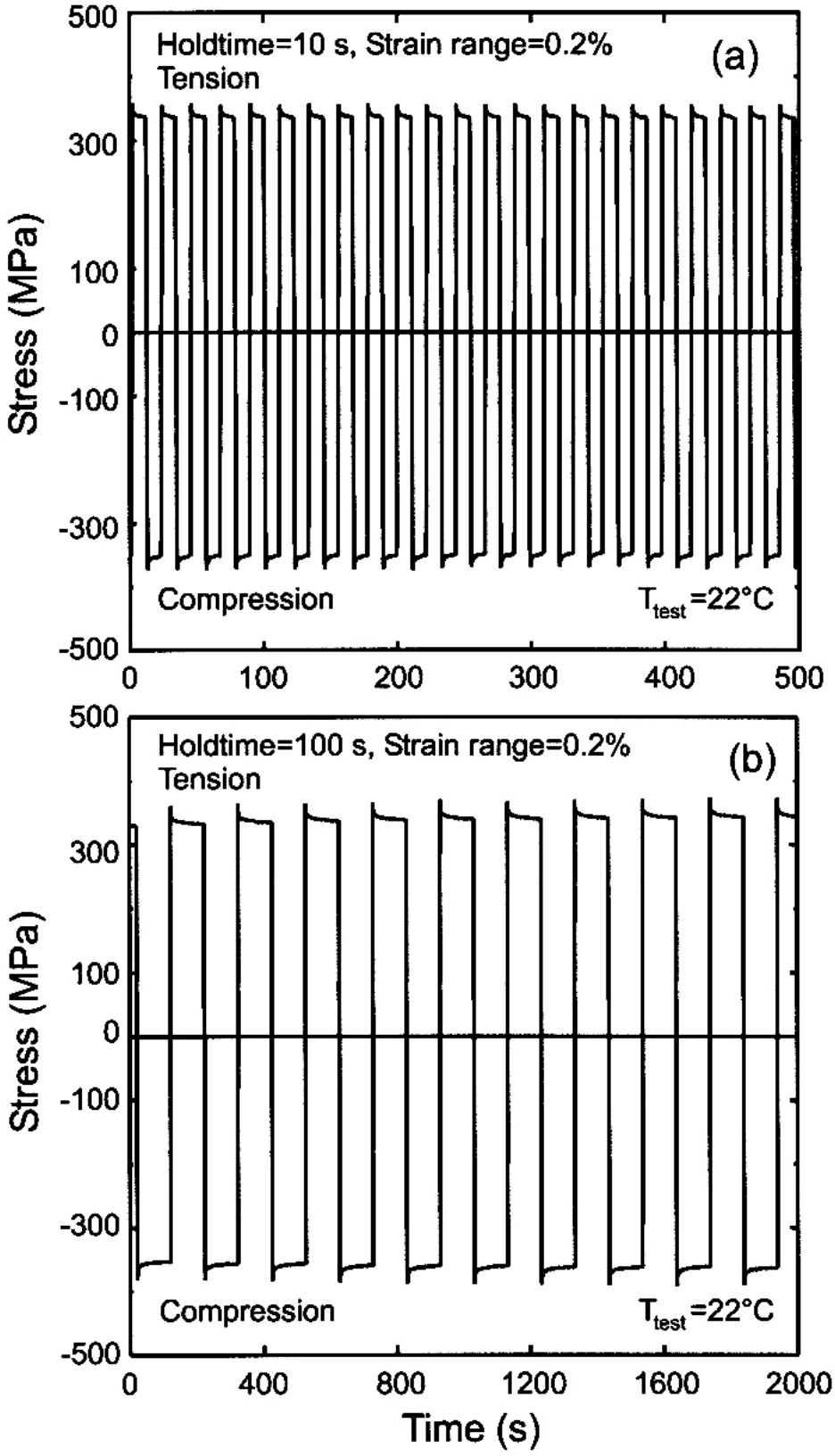

Figure 4. Examples of response of CuCrZr alloy during creep-fatigue tests carried out at 22°C with holdtime of (a) 10 seconds and (b) 100 seconds for a given strain range value of 0.2%.

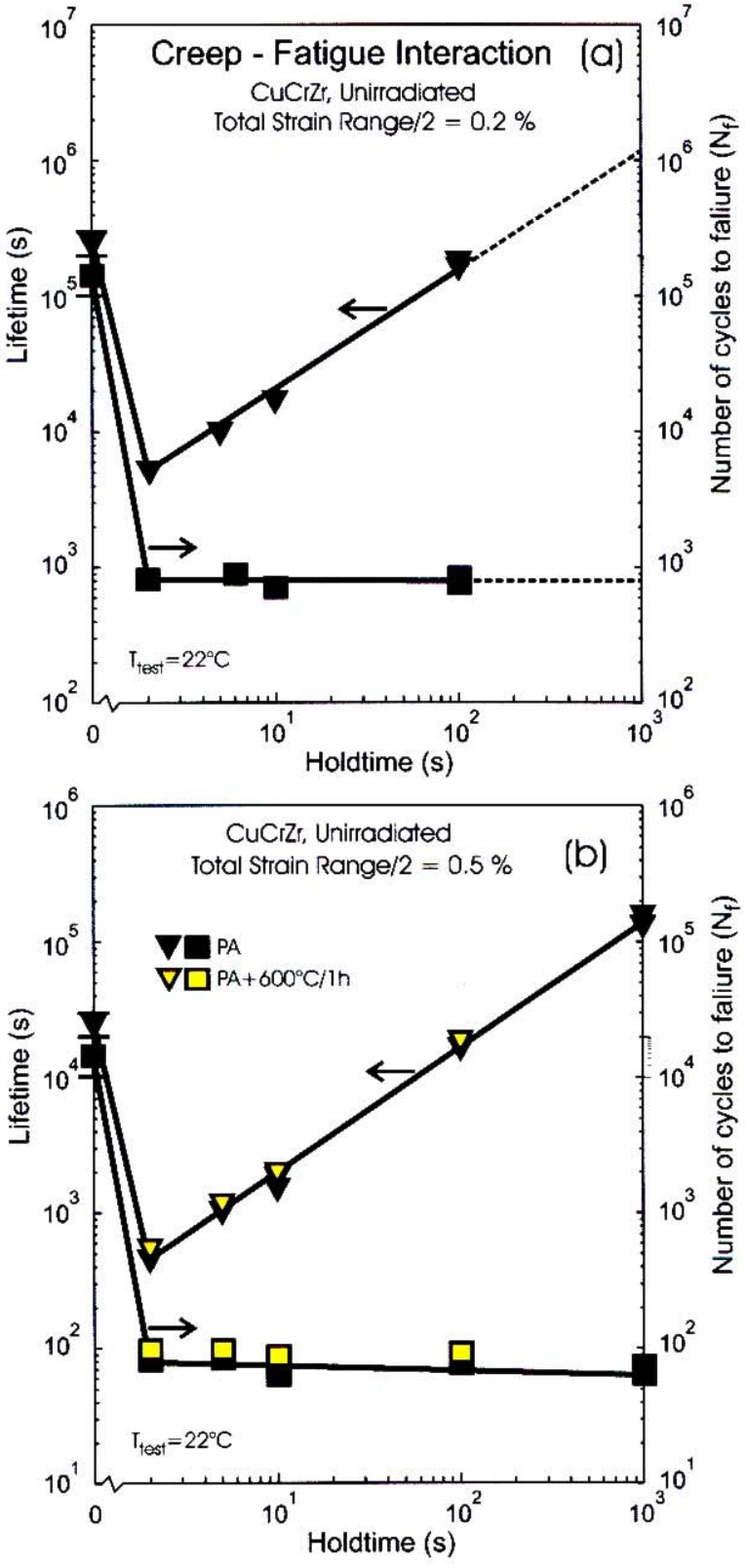

Figure 5. Fracture lifetime and number of cycles to failure as a function of holdtime determined during creep-fatigue tests at 22°C on the unirradiated CuCrZr alloy at strain range values of (a) 0.2% and (b) 0.5%. Note that the annealing at 600°C for 1h after prime ageing does not affect the number of cycles to failure or the lifetime.

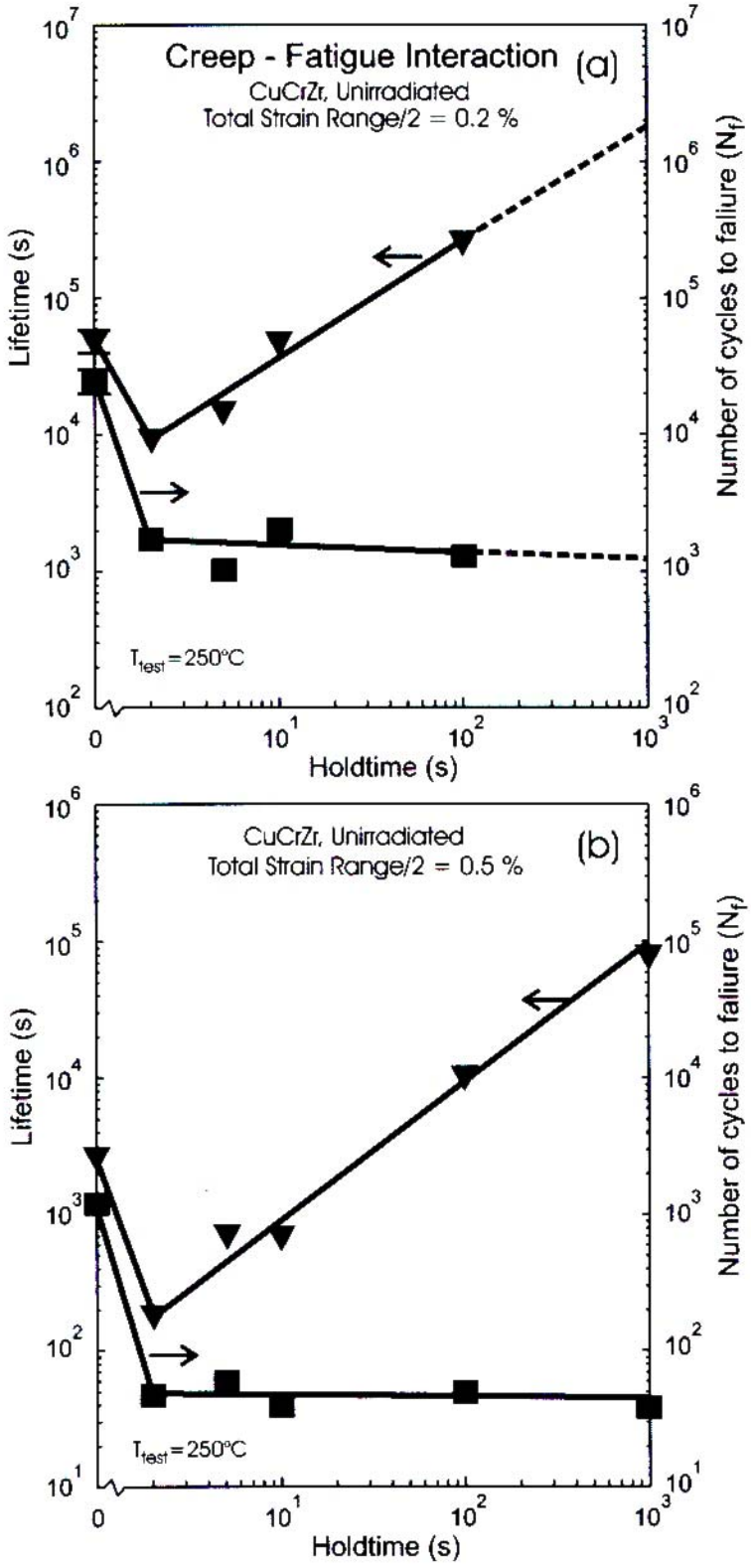

Figure 6. The same as Figure 5, but for tests carried out at 250°C.

The effect of holdtime on the real lifetime of the material and the number of creep-fatigue cycles to failure for the unirradiated and prime aged CuCrZr alloy tested at 22°C is illustrated in Fig. 5 for strain ranges of (a) 0.2% and (b) 0.5%. Fig. 5 (b) also shows the results of CuCrZr specimens that were annealed 600°C for 1h after prime ageing. Results of similar tests carried out at 250°C are shown in Fig. 6 as a function of holdtime. Results shown in Figs. 5 and 6 clearly demonstrate that the number of creep-fatigue cycles to failure is substantially reduced due to application of a holdtime during cyclic loading. The holdtime of even 2 seconds causes a large reduction in the number of cycles to failure both at 22 and 250°C and strain range values of 0.2 and 0.5%. Furthermore, the effect of holdtime increases with decreasing temperature (at a given strain range value) and decreasing strain range value (at a given test temperature). It should be noted, however, that the real lifetime of the material improves at holdtimes of longer than 100 seconds. As can be seen in Fig. 5b, changing the precipitate microstructure by heat treatment after prime ageing (see section 3.2.3) does not seem to modify the effect of holdtime on the number of cycles to failure in any significant way.

3.2.3 Modification of precipitate microstructure in CuCrZr alloy and its impact on tensile properties[3]

B.N. Singh, D.J. Edwards (*Pacific Northwest National Laboratory, Richland, USA) and P. Toft*

Earlier investigations have established that the CuCrZr alloy when irradiated with neutrons in the prime aged condition at temperatures below about 200°C suffers from plastic instability. Experimental results indicate that this may be due to the fact that the precipitates in this alloy in the prime aged condition may be small and, thus, too weak obstacles to dislocation motion during deformation. It was, therefore, decided to coarsen the precipitate size by annealing after prime ageing heat treatment so that the larger and thereby stronger precipitate may prevent the initiation of plastic flow localization by resisting dislocation motion. For this purpose, the post-prime ageing annealing temperature was chosen to be 600°C and a number of specimens were annealed for 1, 2 and 4 hours at 600°C.

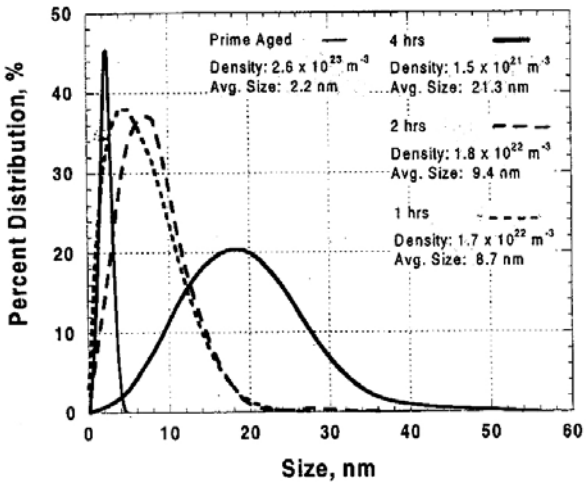

Figure 7. Precipitate size distribution in the unirradiated CuCrZr alloy in the prime aged and in the specimens heat treated (after prime ageing) at 600°C for 1, 2 and 4 hours.

[3] Task TWO-T507-6

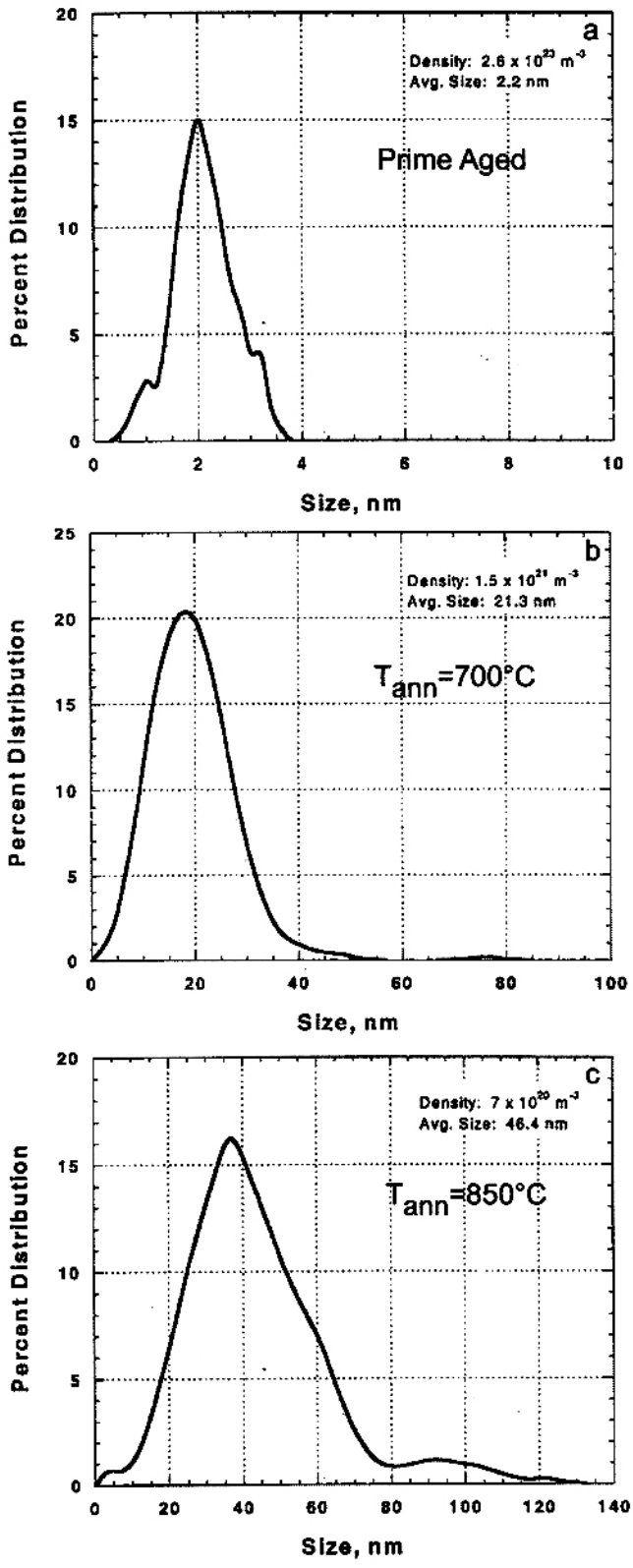

Figure 8. Precipitate size distribution in the unirradiated CuCrZr alloy in the (a) prime aged condition and after annealing at (b) 700°C and (c) 850°C for four hours.

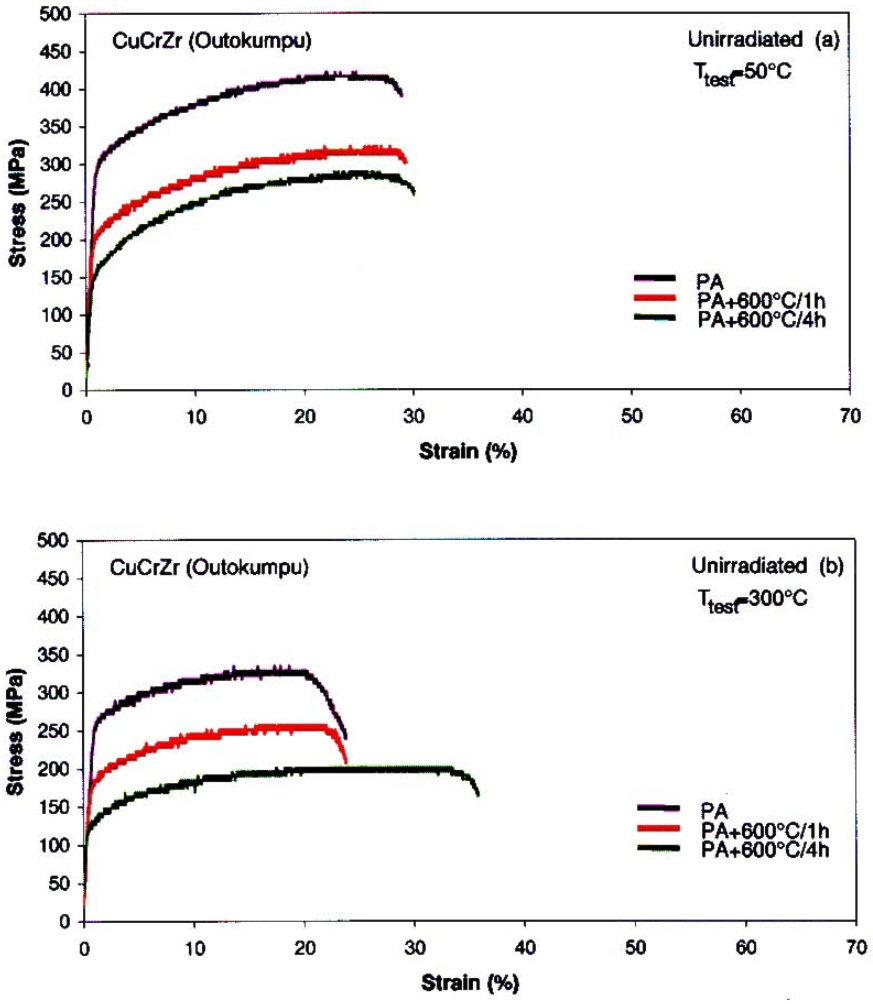

Figure 9. Stress-strain curves for CuCrZr alloy in the prime aged conditioin and after annealing at 600°C for 1 and 4 hours. Tensile tests were carried out at (a) 50°C and (b) 300°C.

Another reason for investigating the effect heat treatment was the uncertainty in the temerature at which copper alloys may be joined to 316 stainless steel while manufacturing the first wall panels. For this reason it was decided to investigate the effect of annealing at 600, 700 and 850°C for four hours after the prime ageing treatment.

After each heat treatment, specimens were examined in a transmission electron microscope and precipitate size and density were determined. The precipitate size distributions for the prime aged specimens and specimens annealed after prime ageing at 600°C for 1, 2 and 4 hours are shown in Fig. 7. As can be seen in Fig. 7, the precipitate density decreases from 2.6 x 10^{23} m^{-3} in the prime aged condition to 1.5 x 10^{21} m^{-3} after annealing at 600°C for 4 hours while the precipitate size increases from 2.2 nm to 21.3 nm. Fig. 8 shows the size distributions for annealing at 600 and 700°C for 4 hours. The annealing at 850°C for 4 hours led to very low density of rather large and heterogeneously distributed precipitates and was, therefore, not measured.

The prime aged (PA) and heat treated specimens were tensile tested at 50 and 300°C. All tests were carried out in vacuum (<10^{-4} torr). Engineering stress-strain curves for the PA and heat treated (at 600°C for 1 and 4 h) specimens tested at 50 and 300°C are shown in Fig. 9.

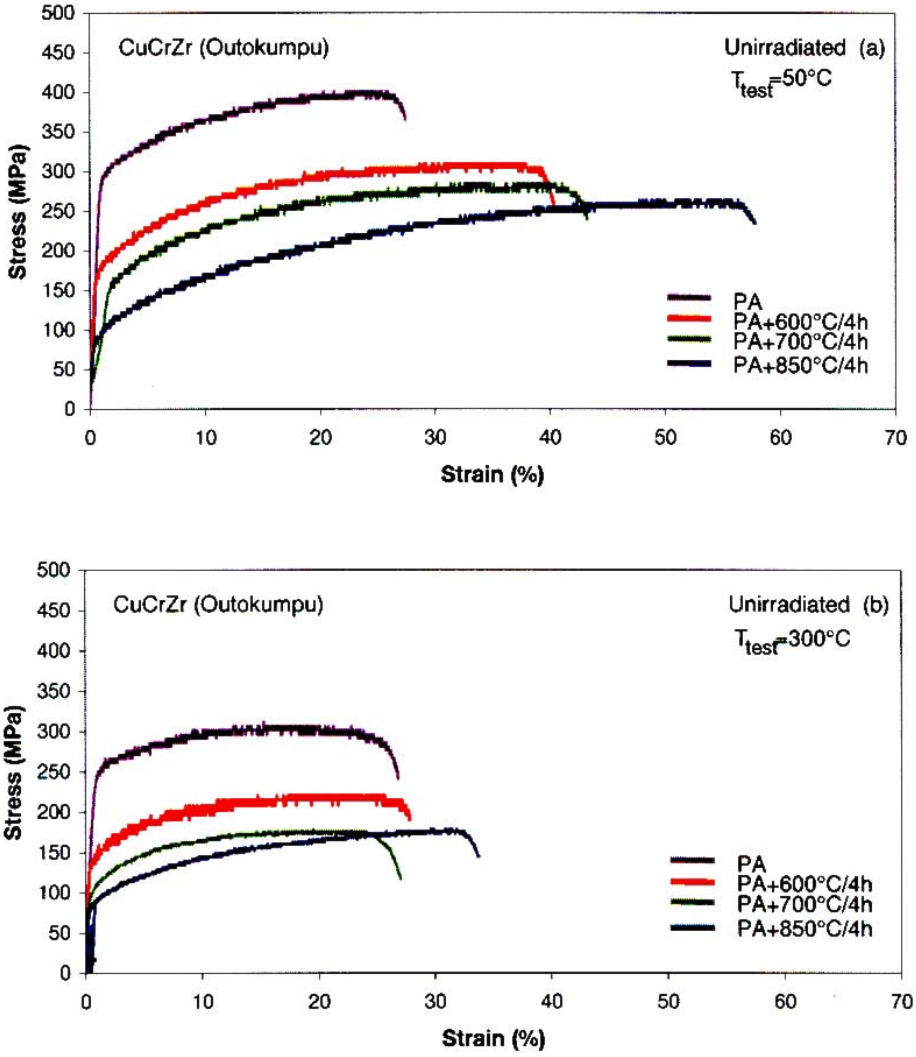

Figure 10. Stress-strain curves for CuCrZr alloy heat treated (after prime ageing) at 600, 700 and 850°C for 4h. The tensile tests were carried out at (a) 50°C and (b) 300°C.

Both at 50 and 300°C, the tensile strength decreases with decreasing precipitate density (see Fig. 7). Tensile results for the PA and heat treated specimens at 600, 700 and 800°C for 4 h and tested at 50 and 300°C are shown in Fig. 10. Results clearly show that precipitate coarsening increases with increasing temperature (see Fig. 8) and, therefore, the tensile strength decreases with the annealing.

3.3 Long-term technology

3.3.1 Dose dependence of defect accumulation[4]

M. Eldrup, B. N. Singh, S. J. Zinkle, T.S. Byun* and K. Farrell* (*Metals and Ceramics Division, Oak Ridge National Laboratory, Oak Ridge, USA)*

In order to investigate the difference in defect accumulation between fcc Cu and bcc Fe, tensile specimens were neutron irradiated at ~70°C in the HFIR reactor at Oak Ridge

National Laboratory to fluences in the range of 7.2×10^{20} - 4.7×10^{24} n/m^2 (E > 1 MeV) corresponding to displacement dose levels in the range of 0.0001 - 0.8 dpa in copper and 0.0001 - 0.72 dpa in iron. Irradiated specimens were characterized using positron annihilation spectroscopy, transmission electron microscopy and electrical conductivity measurements. A limited number of iron specimens irradiated to different dose levels were tensile tested at 70°C.

The results clearly showed a difference in defect accumulation between copper and iron during neutron irradiation in a wide dose range. In Cu, no void nucleation was observed. In Fe at 10^{-4} dpa a low density of very small vacancy clusters (1 - 3 vacancies) were detected while voids and/or micro-voids were observed at doses of 0.0009 dpa and above. Both the density and the average size increase with dose. Figure 11 shows the dose dependence of the cavity density in Fe as determined by positron annihilation spectroscopy (PAS) compared with the cluster density in Cu and Fe. The average size increased from about 0.3 nm to about 0.6 nm in the dose range 0.0001 - 0.23 dpa. In TEM, voids become visible only in the specimen irradiated to 0.72 dpa. The density was of the order of 10^{24} m^{-3} in the size range below 1.5 nm in agreement with the PAS estimates. The PAS data for iron suggested that the swelling rate is constant (~4±2 %/dpa) for doses below 0.01 dpa, but decreases to ~ 0.2 %/dpa at 0.23 dpa. It is interesting to note that this behaviour is similar to that observed in copper irradiated at 250°C.

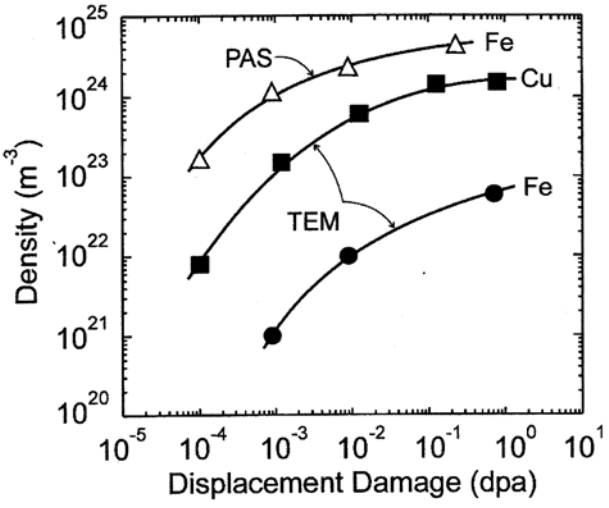

Figure 11. Dose dependence of cluster density in copper and iron irradiated at 70°C. In copper (■) the clusters are mainly SFTs. In iron the TEM results (●) are mainly densities of SIA clusters while PAS results (▲) are for 3-dimensional vacancy clusters (voids).

[4] Task TTMS-001

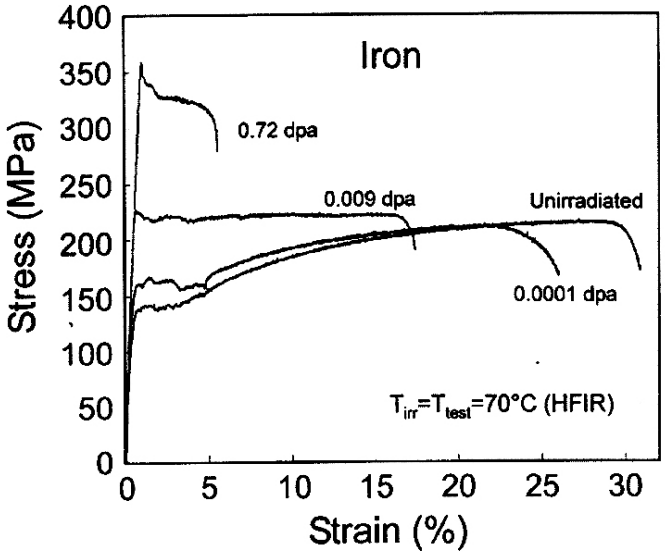

Figure 12. Stress-strain curves for pure iron irradiated at ~70°C to different dose levels and tensile tested at 70°C. Note the increase in yield strength and decrease in work hardenability and uniform elongation with increasing dose level. The flow localization and plastic instability is very marked at 0.72 dpa.

TEM investigations showed that the density of SIA clusters in Fe increases with dose. At doses higher than ~ 0.01 dpa, the clusters begin to segregate and coalesce leading to formation of rafts of SIA clusters. The formation of the raft-like structure is significantly more efficient in bcc iron than in fcc copper.

The mechanical properties were also found to depend on irradiation dose. Figure 12 shows an increase in the yield stress and a decrease in the uniform elongation as a function of increasing dose level in iron.

In addition to the microstructural information, the present work demonstrates that positron annihilation spectroscopy can provide valuable information about the microstructure of irradiated metals, in particular about the presence of submicroscopic voids.

3.3.2 Dislocation decoration with interstitial clusters in bcc iron[5]

N.M. Ghoniem, S.-H. Tong*, J. Huang*, B.N. Singh and M. Wen**
*(*University of California, Los Angeles, USA),*

It is well known that neutron irradiation of metals and alloys at temperatures below the recovery stage V (about 0.3 T_m for iron where T_m is the melting temperature in Kelvin) causes a substantial increase in the yield strength and a significant decrease in the ductility (see 3.3.1, Fig. 11). It is the decrease in the ductility and occurrence of plastic instability due to plastic flow localization which is a matter of serious concern from the point of view of application of materials in a fission or fusion reactor environment. Recently, the cascade induced source hardening (CISH) model has been proposed to rationalize this phenomenon[6]. The model is based on the premise that during irradiation under cascade damage conditions, the grown in dislocations get decorated with an atmosphere of small interstitial clusters and that this atmosphere prevents the grown-in dislocations from acting as dislocation sources. Later, it

[5] Task TTMS-001
[6] B.N. Singh, A.J.E. Foreman and H. Trinkaus, J. Nucl. Mater. 251 (1997) 103

was shown analytically using isotropic elasticity theory that such decoration is likely to occur by 1-D diffusing interstitial clusters produced in the cascades.

In order to verify the main conclusions of the analytical calculations and to gain further insight into the processes involved, a combination of Kinetic Monte Carlo and 3-D Dislocation Dynamics computational techniques have been employed to study the phenomenon of dislocation decoration in bcc iron. To study how glissile interstitial clusters migrate and interact amongst themselves and with the internal stress fields of the grown-in dislocations, a computational box of 400a x 400a x 400a ('a' is the lattice constant of bcc iron) is used with periodic boundary conditions. In order to study dislocation-cluster interaction and the decoration process, a dislocation loop lying on the $<0\bar{1}1>$ plane with Burgers vector $\frac{1}{2}<\bar{1}11>$ is introduced into the simulation box. A number of interstitial clusters (of density varying in the range of $5 \times 10^{22} - 2 \times 20^{23}$ m^{-3}) are introduced in the box with a random distribution and their initial jump directions are also randomly specified. The interstitial clusters are then allowed to diffuse one-dimensionally and interact amongst themselves and the grown-in dislocation loop (Fig. 13). When a cluster approaches the dislocation at distances closer than the "stand-off" distance (taken as 1.5 nm), the cluster is stopped. As can be seen in Fig. 13, the grown-in dislocation loop get decorated by the interstitial clusters in a very short time (6 ns).

Another interesting feature of these interactions (loop-loop and loop-dislocation) is that when clusters are within a distance of several nanometers from each other, and have their Burgers vector in parallel directions, will trap one another and form a raft of loops. The formation of rafts of loops is well known experimentally in bcc metals.

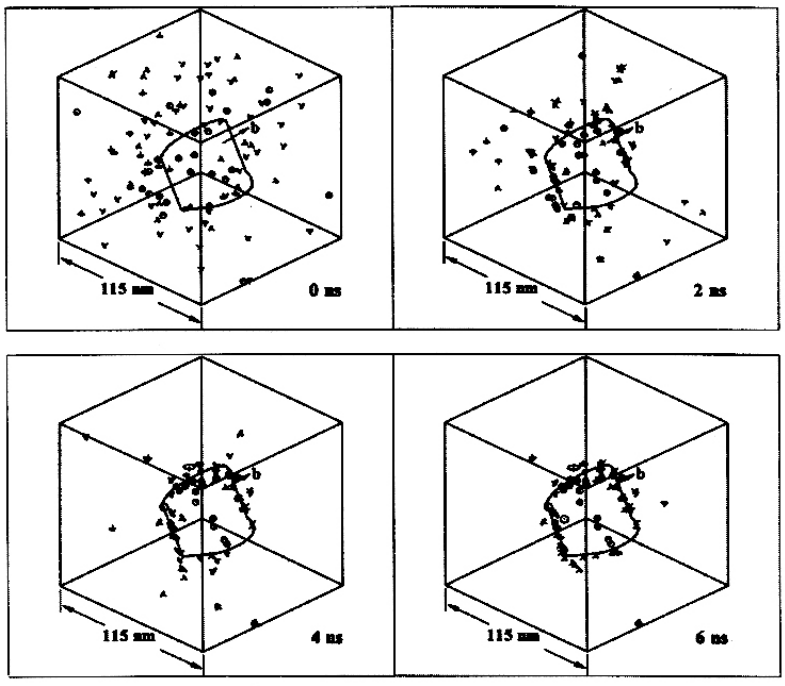

Figure 13. KMC simulation of dislocation decoration during irradiation producing glissile SIA clusters. A randomly distributed population of SIA clusters are allowed to diffuse and cluster in the stress field of a 3-D dislocation loop. As can be seen, the grown-in dislocation gets decorated by SIA clusters in a very short time.

3.3.3 Radiation hardening in bcc iron[7]

B.N. Singh, M. Eldrup. N.M. Ghoniem and M. Wen**
*(*University of California, Los Angeles, USA)*

It has been shown experimentally that neutron irradiation causes a substantial amount of hardening in bcc iron at 50 and 100°C. However, for a given irradiation temperature (homologous) the displacement dose level is considerably lower in bcc iron than that in fcc copper. Experiments have also demonstrated that irradiation at these temperatures produces a high density of hardening obstacles in the form of nano-size voids in bcc iron and nano-size stacking fault tetrahedral (SFTs) in fcc copper. In both cases, the phenomena of yield drop and plastic flow localization in the form of cleared channels are observed. This is interpreted to mean that in both cases CISH model can be approximately applied to understand the magnitude of hardening and the occurrence of plastic flow localization.

In the present work, the magnitude of hardening due to irradiation has been calculated within the framework of CISH model using the 3-D Dislocation Dynamics and Kinetic Monte Carlo (KMC) procedures. In the case of bcc iron, the main obstacles to dislocation motion are taken to be the nano-size voids. The density of these obstacles on the glide plane is calculated from the experimentally measured values of the volumetric density of nano-size voids in pure iron neutron irradiated at 50 and 100°C to different dose levels. According to the CISH model a large number of dislocation sources are activated at the upper yield stress. These newly generated dislocations move on the glide planes and encounter the obstacles randomly distributed on the glide planes. Each dislocation segment is represented by a circular arc, and its curvature is determined by the applied stress, sum of all interaction forces and Burgers vector. When a dislocation segment encounters the nearest obstacle it splits into two segments and each segment continues to move until it reaches its equilibrium curvature or when the angle between the two tangents at the obstacle reaches a critical value, Φ_c. A KMC procedure is implemented to determine the probability of destruction of nanovoids. This is calculated from the height of the energy barrier, the work done by the local forces at tangent points and the lattice temperature. After the annihilation of the nanovoids, these two segments merge into one and the unified segment is advanced till it meets the next obstacle on the glide plane. Using this procedure, the stress level at the lower yield stress is obtained. The main results of these calculations are summarized in Fig. 14 for pure bcc iron neutron irradiated at 50 and 100°C to different dose levels. For comparison experimental results are also plotted in Fig. 14. The agreement between the calculated and the experimental results is reasonably good. The calculated results are somewhat lower probably because the effect of interstitial clusters is not included in the calculations.

[7] Task TTMS-001

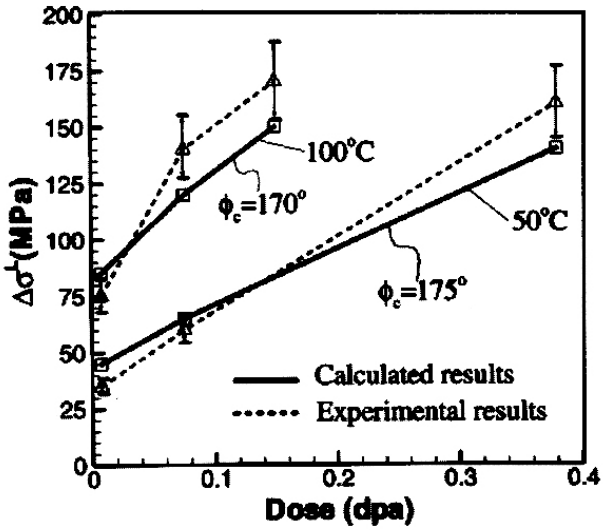

Figure 14. Experimental and calculated dose dependencies of irradiation induced increase in the lower yield stress in pure bcc iron neutron irradiated at 50 and 100°C. Note that the calculated trend showing increase in hardening with increasing dose level is in good accord with experimentally measured trend.

3.4 Underlying technology

3.4.1 The effects of one-dimensional migration of self-interstitial clusters on the formation of void lattices

H.L. Heinisch (*Pacific Northwest National Laboratory, Richland, USA) and B.N. Singh*

Void lattices in irradiated metals were first observed about 30 years ago, and while they have been the subject of many theoretical and experimental studies since then, no definitive theory of void lattice formation exists. Crowdion clusters having the property of three-dimensional diffusion in the material along paths consisting of segments of one-dimensional random walks are central to the Production Bias Model of void swelling[8], which has been shown to be quite successful in describing many aspects of microstructure evolution under cascade-producing irradiation. The rationale for the present investigation is that if a theory can explain void swelling, then it should also be compatible with the formation of void lattices. Thus, a key element of the Production Bias Model, the one-dimensional migration of crowdion clusters with occasional Burgers vector changes, was examined as a necessary condition for the formation of a void lattice.

Kinetic Monte Carlo computer experiments were performed with a simple model for the interactions of vacancy and SIA defects with voids in which the average length of the 1-D migration path segments of SIA clusters is the variable quantity. A cubic test cell containing an atomic-scale, face-centered cubic lattice was used. The cell contained spherical voids and mobile defect clusters, each defect being associated with a lattice site of the underlying crystal structure. The mobile clusters consisted of identically sized crowdion and vacancy clusters. Each crowdion cluster migrated in a 1-D random walk along a randomly chosen

[8] S.I. Golubov, B.N. Singh and H. Trinkaus, J. Nucl. Mater. 276 (2000) 78

close-packed direction (<110>) on the fcc crystal lattice for exactly n_{dc} jumps before randomly choosing the close-packed direction for its next random walk of n_{dc} jumps. The vacancy clusters migrated by 3-D random walks on the fcc crystal lattice. The KMC modeling was used to investigate the role of 1-D migration and the effects of Burgers vector changes on the "shadow effect," whereby voids aligned along close-packed directions shield each other from 1-D migrating SIA defects. The strength of the shadow effect was investigated in a series of KMC experiments. A lattice of 256 uniform-sized voids in the test cell described above was supplemented by 256 additional voids of the same size placed at random positions within the cell. The cell was then "irradiated" with 50,000 crowdion clusters placed randomly in the cell and executing 1-D random walks along the close-packed directions, each for n_{dc} jumps before selecting a new Burgers vector direction. There were no mobile vacancy clusters in this experiment. Runs were done with different values of n_{dc}. Figure 15a shows the initial configuration looking down the [001] direction of the cubic volume. Figure 15b shows the same view after irradiation by the crowdion clusters with n_{dc}= 1 jump, the condition for "pure 3-D" migration. The lattice voids and random voids were attacked equally by the crowdion clusters. Figures 15c and 15d show the results for n_{dc} = 500 jumps and n_{dc} = 5000 jumps, respectively. The average 1-D path length for 500 jumps is about 0.85 times the nearest neighbor distance of voids in the lattice, while that for 5000 jumps is 2.7times. The effect of shadowing is quite strong, even when the 1-D path length is of modest size and leads to an almost perfect void lattice (Fig. 15d).

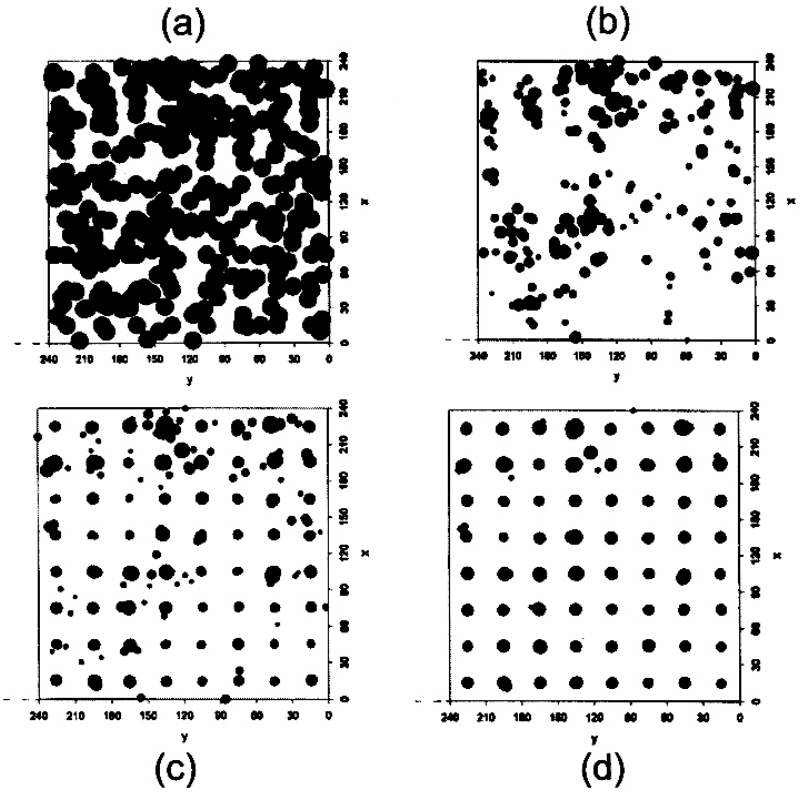

Figure 15. Ordering of voids in a fcc crystal lattice in a cubic test cell containing 256 voids in a lattice and 256 randomly placed voids. The test cell was irradiated with 50,000 interstitial clusters diffusing one-dimensionally for different values of n_{dc} (is the number of jumps that a 1-D diffusing interstitial cluster makes before it changes the direction of diffusion and makes another n_{dc} jump in that new direction): (a) initial spatial distribution of voids, (b) n_{dc} = 1 (representing effective 3-D diffusion), (c) n_{dc} = 500 (~0.85 of the nearest neighbour distance of the void lattice) and (d) n_{dc} = 5000 (2.7 times the nearest neighbour distance).

KMC computer experiments were also performed to test the size stability, whether the voids grow or shrink, as a function of the value of n_{dc}. A lattice of 256 voids in a cell, as described above, was irradiated with equal numbers of crowdion clusters and vacancies. It was found that, under the condition of equal numbers of vacancies and interstitials available to interact with the voids, the size stability of voids in the lattice could be maintained when SIA clusters have 1-D path lengths on the order of the void lattice spacing.

Based on the results of these studies, the shadow effect is very strong, and it does not require 1-D path lengths significantly greater than the void lattice spacing for crowdion clusters to be effective in selecting a void lattice, relative to random voids. Of course, the shadow effect is much stronger if the crowdion clusters have longer 1-D path lengths, but under those conditions the fraction of crowdions available for interacting with the voids becomes much smaller. To maintain the void size under the long 1-D path length conditions requires that the available SIA in crowdion clusters must outnumber the available 3-D migrating vacancies by a large factor (about a factor of 7 in the example here). However, under the actual conditions in real materials, crowdion clusters with very long 1-D path lengths are probably rare. Thus, it should be possible to maintain a void lattice when the average 1-D path lengths of a significant fraction of crowdion clusters is on the order of the void lattice spacing. Further KMC computer experiments will be aimed at determining the conditions for void lattice formation.

3.4.2 Dislocation-loop interaction in fcc copper[9]

Yu. N. Osetsky , D.J. Bacon* (*The University of Liverpool, Liverpool, U.K.), A. Serra** (**Universitat Politècnica de Catalunya, Barcelona, Spain) and B.N. Singh*

The most important feature of the primary damage produced by energetic neutrons is the production of both sessile and highly glissile clusters of self-interstitial atoms (SIAs). The one-dimensional transport of SIA clusters leads to spatial segregation of interstitials and vacancies and is responsible for dislocation decoration and formation of rafts of loops. This forms the basis of the CISH model for describing the phenomena of radiation hardening, yield drop and plastic flow localization. Furthermore, it is also the segregation of SIAs and vacancies which gives rise to an excess of vacancies responsible for void nucleation and growth (i.e. void swelling) and is used as the main driving force in the Production Bias Model (PBM)[9]. In all these cases loop-loop and dislocation-loop interactions play a crucial role. While using the CISH model to calculate the magnitude of hardening either analytically or in terms of 3-D dislocation dynamics (see section 3.3.3) or using the PBM to estimate void swelling, the strength of these interactions are calculated in terms of isotropic linear elasticity theory. It is not clear, however, as to whether or not the strength of these interactions can be obtained accurately enough within the framework of elasticity theory. To eliminate this uncertainty, atomistic calculations have been carried out to determine the strength of interaction between an edge dislocation and a SIA loop containing 49 SIAs in fcc copper.

Molecular statics were used to study the cluster-dislocation interaction energy at a temperature of zero Kelvin in fcc copper lattice. A crystallite of about a million atoms was oriented along $[1\bar{1}0]$, $[11\bar{2}]$ and [111] directions. The size along the Burgers vector, b, was approximately 15 nm along the dislocation line. An isolated dislocation was first introduced and relaxed. A cluster with the same Burgers vector as that of the edge dislocation was then

[9] B.N. Singh, S.I. Golubov, H. Trinkaus, A. Serra, Yu. N. Osetsky and A.V. Barashev, J. Nucl. Mater. 251 (1997) 107

created at a certain distance, $r_{<111>}$ (i.e. along [111] direction for the copper crystallite) below the dislocation slip plane and the crystallite was relaxed again.

The dislocation-cluster interaction energy was calculated using the energies of the previously rerlaxed isolated dislocation and a cluster. The interatomic interactions were described by manybody potentials. The interaction energy, E_{INT}, thus obtained was compared with the results of calculations using the full isotropic elasticity and the simple infinitesimal loop approximation. The results are compared in Fig. 16. The results show that the interaction between the dissociated edge dislocation and a cluster in copper is complicated since the stress field of the dislocation enhances the dissociation of SIA clusters. As a result, the interaction energy is significantly higher at short distances. However, for long-range interactions, when cluster-dislocation separation is much larger than the cluster size, the elasticity calculations yield good results particularly when the dislocation core energy and radius are obtained from atomistic calculations.

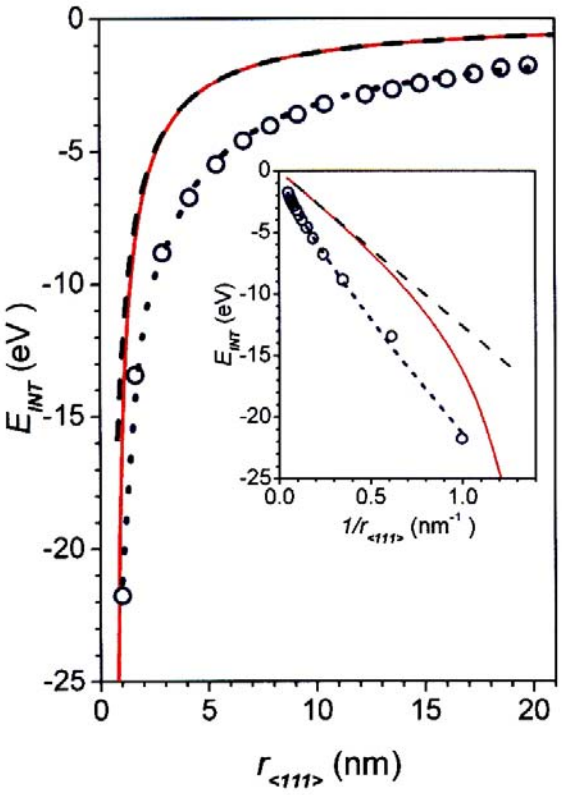

Figure 16. Interaction energy between ½ <110> dislocation ½ <110> interstitial cluster containing 49 SIAs. Black dashed line – infinitesimal loop approximation, solid red line – full integral of dislocation stress field over loop perimeter, blue circles – results of the molecular static calculation, blue dotted line – interpolation of calculated results by power function of distance $E_{INT} = -21.35\ r^{-0.82}$ eV. Note that the exponent is –1 for the infinitesimal loop and long-range full integral.

3.4.3 Void nucleation under cascade damage condition

H. Trinkaus (*Forschungszentrum Jülich, Jülich, Germany) and B.N. Singh*

The problem of void nucleation has been a subject of studies since the early 1970s. In these studies the main driving force for void nucleation, the vacancy supersaturation, was assumed to be constant in the steady-state and was taken to arise due to the preferential absorption of self-interstitial atoms (SIAs) by dislocations ("dislocation bias"). Unfortunately, these earlier theoretical treatments were unable to rationalize the experimental results. In the early 1990s, it was recognized that in fact the origin of vacancy supersaturation under cascade damage conditions was intrinsically related to the intracascade clustering of SIAs and the properties of these clusters. This led to the concept of production bias[10,11] and later became known as Production Bias Model (PBM). Since then a considerable amount of effort has been made in validating the model both theoretically and experimentally. It has been shown conclusively that experimental results which could not be explained by earlier theories could now be rationalized within the framework of the PBM. However, so far the PBM was used to treat the problems of void growth and void swelling but not the void nucleation.

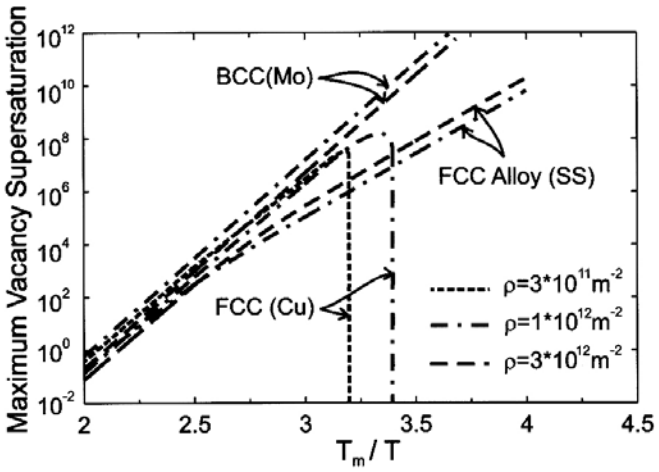

Figure 17. Vacancy supersaturation calculated using PBM as a function of reciprocal homologous temperature for bcc (Mo), fcc (Cu) and fcc alloy (austenitic stainless steel) under neutron irradiation conditions for three dislocation densities (ρ).

Recently, theoretical work has been initiated to address the problem of void nucleation in metals and alloys in terms of the PBM. The present approach utilizes the results of controlled experiments as well as the results of molecular dynamics calculations regarding the details of the primary damage production and properties of the clusters produced in the cascades. As a first attempt, we have calculated the evolution of vacancy supersaturation as a function of irradiation temperature and displacement dose. The results for bcc molybdenum, fcc copper and fcc austenitic stainless steel are shown in Figs. 17 and 18, respectively for different dislocation densities. It should be pointed out that under cascade damage conditions, both the temperature and the dose dependencies of vacancy supersaturation during void nucleation is dominated by the production bias. Furthermore, both the temperature and dose dependencies of the vacancy supersaturation are qualitatively consistent with the experimental results on void density as a function of irradiation temerature and displacement dose levels.

[10] C.H. Woo and B.N. Singh, Philos. Mag. A65 (1992) 889.
[11] B.N. Singh and A.J.E. Foreman, Philos. Mag. A66 (1992) 975

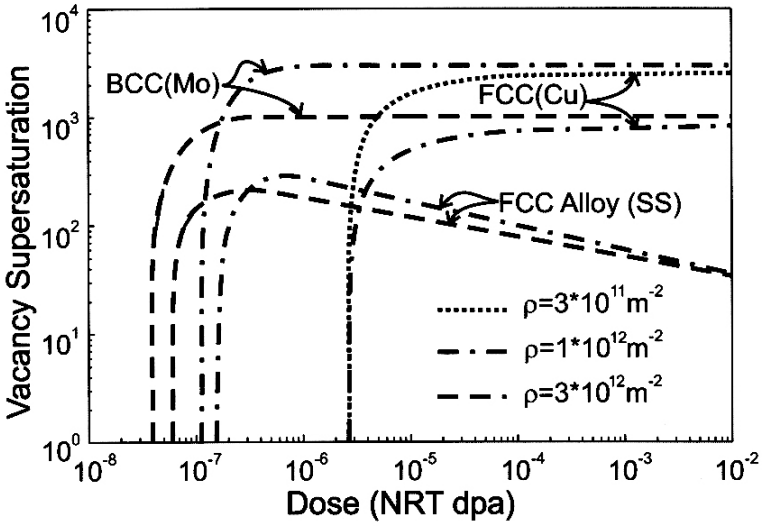

Fig. 18. The same as in Fig. 17 but as a function irradiation dose level for an irradiation temperature of 0.4 T_m (T_m is the melting temperature).

3.5 Publications and conference contributions

3.5.1 International publications

Eldrup, M.; Singh, B.N., Void nucleation in fcc and bcc metals: A comparison of neutron irradiated copper and iron. 12. International conference on positron annihilation - ICPA-12, München (DE), 6-12 Aug 2000. Mater. Sci. Forum (2001) v. 363-365 p. 79-81

Ghoniem, N.M.; Tong, S.H.; Singh, B.N.; Sun, L.Z., On dislocation interaction with radiation-induced defect clusters and plastic flow localization in fcc metals. Phil. Mag. A (2001) v. 81 p. 2743-2764

Golubov, S.I.; Ovcharenko, A.M.; Barashev, A.V.; Singh, B.N., Grouping method for the approximate solution of a kinetic equation describing the evolution of point-defect clusters. Phil. Mag. A (2001) v. 81 p. 643-658

Golubov, S.I.; Singh, B.N.; Trinkaus, H., On recoil-energy-dependent defect accumulation in pure copper. Part 2. Theoretical treatment. Phil. Mag. A (2001) v. 81 p. 2533-2552

Schiøtz, J.; Leffers, T.; Singh, B.N., Dislocation nucleation and vacancy formation during high-speed deformation of fcc metals. Phil. Mag. Lett. (2001) v. 81 p. 301-309

Singh, B.N.; Edwards, D.J.; Eldrup, M.; Toft, P., Effect of bonding and bakeout thermal cycles on the properties of copper alloys irradiated at 350 deg. C. J. Nucl. Mater. (2001) v. 295 p. 1-15

Singh, B.N.; Edwards, D.J.; Toft, P., Effect of neutron irradiation and post-irradiation annealing on microstructure and mechanical properties of OFHC-copper. J. Nucl. Mater. (2001) v. 299 p. 205-218

Tähtinen, S.; Laukkanen, A.; Singh, B.N., Investigations of copper to stainless steel joints. Fusion Eng. Des. (2001) v. 56/57 p. 391-396

Zrubcova, J.; Kristiak, J.; Batsberg Pedersen, W.; Pedersen, N.J.; Eldrup, M., Light effects of positronium formation in polymers. 12. International conference on positron annihilation - ICPA-12, München (DE), 6-12 Aug 2000. Mater. Sci. Forum (2001) v. 363-365 p. 359-361

3.5.2 Danish reports

Eldrup, M.; Singh, B.N., Investigations of void formation in neutron irradiated iron and F82H steel. Risø-R-1241 (EN) (2001) 21 p.

Lynov, J.P.; Singh, B.N (eds.), Association Euratom - Risø National Laboratory annual progress report 1999. Risø-R-1245(EN) (2001) 48 p.

Lynov, J.P.; Singh, B.N (eds.), Association Euratom - Risø National Laboratory annual progress report 2000. Risø-R-1283(EN) (2001) 45 p.

Singh, B.N.; Edwards, D.J.; Toft, P., Microstructure and mechanical properties of neutron irradiated OFHC-copper before and after post-irradiation annealing. Risø-R-1213(EN) (2001) 29 p.

Singh, B.N.; Eldrup, M.; Zinkle, S.J.; Golubov, S.I., On grain size dependent void swelling in pure copper irradiated with fission neutrons. Risø-R-1190(EN) (2001) 28 p.

Singh, B.N.; Stubbins, J.F.; Toft, P., Impact of creep-fatigue interaction on the lifetime of a dispersion strengthened copper alloy in unirradiated and irradiated conditions. Risø-R-1253(EN) (2001) 30 p.

Singh, B.N.; Tähtinen, S., Final report on characterization of physical and mechanical properties of copper and copper alloys before and after irradiation. Risø-R-1276 (EN) (2001) 21 p.

3.5.3 Foreign books and reports

Edwards, D.J.; Singh, B.N.; Toft, P., True stress-strain behaviour of as-irradiated and post-irradiation annealed pure copper. Fusion Materials Semiannual Progress Report, DOE/ER-0313/30, June 30, (2001) 99-108.

Heinisch, H.L.; Singh, B.N., The effects of one-dimensional migration of self-interstitial clusters on the formation of void lattices. Fusion Materials Semiannual Progress Report, DOE/ER-0313/31, December 31, ((2001) 161-163.

Edwards, D.J.; Singh, B.N., Overageing of Outokumpu CuCrZr at 600^{o}C. Fusion Materials Semiannual Progress Report, DOE/ER-0313/31, December 31, (2001) 118-122.

Singh, B.N.; Trinkaus, H.; Golubov, S.I., Radiation damage in crystalline solids: Theory. In: Encyclopedia of materials: Science and technology. Vol. 8., Buschow, K.H.J.; Cahn, R.W.; Flemings, M.C.; Ilschner, B.; Kramer, E.J.; Mahajan, S. (eds.), (Pergamon, Oxford, 2001) p. 7957-7972.

3.5.4 Unpublished conference contributions and lectures

Edwards, D.J.; Singh, B.N., Dislocation channeling in irradiated materials: Relationship between microstructure and onset of localized flow. 2001 MRS Spring meeting. Symposium BB: Material instabilities and patterning in metals, San Francisco, CA (US), 17-18 Apr 2001. Unpublished.

Edwards, D.J.; Singh, B.N.; Xu, Q.; Toft, P., Post-irradiation annealing of neutron irradiated CuCrZr: Changes in microstructure and mechanical properties. 10. International conference on fusion reactor materials (ICFRM 10), Baden-Baden (DE), 14-19 Oct 2001. Unpublished. Abstract available

Eldrup, M.; Singh, B.N.; Zinkle, S.J.; Byun, T.S.; Farrell, K., A comparison of neutron irradiated copper and iron: Effects of radiation dose and annealing. 10. International conference on fusion reactor materials (ICFRM 10), Baden-Baden (DE), 14-19 Oct 2001. Unpublished. Abstract available

Ghoniem, N.M.; Tong, S.H.; Huang, J.; Singh, B.N., New insights into dislocation-defect interaction from large-scale computer simulations. 10. International conference on fusion reactor materials (ICFRM 10), Baden-Baden (DE), 14-19 Oct 2001. Unpublished. Abstract available

Ghoniem, N.M.; Tong, S.H.; Singh, B.N.; Huang, J., Radiation hardening and the dynamics of dislocation-defect interaction in iron: A comparison between theory and experiment. 10. International conference on fusion reactor materials (ICFRM 10), Baden-Baden (DE), 14-19 Oct 2001. Unpublished. Abstract available

Heinisch, H.L.; Singh, B.N., The effects of one-dimensional migration of self-interstitial clusters on the formation of void lattices. 10. International conference on fusion reactor materials (ICFRM 10), Baden-Baden (DE), 14-19 Oct 2001. Unpublished. Abstract available

Kalinin, G.; Fabritziev, S.; Singh, B.; Tähtinen, S.; Zinkle, S., Specification of properties and design allowables for copper alloys used in HHF components of ITER. 10. International conference on fusion reactor materials (ICFRM 10), Baden-Baden (DE), 14-19 Oct 2001. Unpublished. Abstract available

Osetsky, Y.N.; Bacon, D.J.; Singh, B.N.; Wirth, B., Atomistic study of interaction, accumulation and annihilation of cascade induced defect clusters. 10. International conference on fusion reactor materials (ICFRM 10), Baden-Baden (DE), 14-19 Oct 2001. Unpublished. Abstract available

Osetsky, Y.N.; Bacon, D.J.; Singh, B.N., Statistical analysis of cluster production efficiency in md simulaiton of cascades in copper. 10. International conference on fusion reactor materials (ICFRM 10), Baden-Baden (DE), 14-19 Oct 2001. Unpublished. Abstract available

Singh, B.N., Status, focus and priority issues of fusion materials programs. International Energy Agency fusion materials modeling workshop, San Francisco, CA (US), 20-21 Apr 2001. Unpublished.

Singh, B.N., Modeling of helium effects in high and low temperature regimes. International Energy Agency fusion materials modeling workshop, San Francisco, CA (US), 20-21 Apr 2001. Unpublished.

Singh, B.N., Radiation hardening and plastic flow localization under cascade damage conditions. Seminar at Department of Mechanical and Aerospace Engineering, UCLA, Los Angeles, CA (US), 25 Apr 2001. Unpublished.

Singh, B.N., The influence of neutron irradiation on microstructure and properties of copper and copper alloys. Workshop on irradiation damage and oxidation in copper and copper alloys, VTT Manufacturing Technology, Otaniemi (FI), 28 May 2001. Unpublished.

Singh, B.N., Particle-solid interactions and materials response. Annual fusion seminar, Espoo (FI), 28 May 2001. Unpublished.

Singh, B.N., Radiation hardening and plastic flow localization in pure Fe and Cu. Workshop on damage production, accumulation and consequences, Liverpool (GB), 6-7 Aug 2001. Unpublished.

Singh, B.N., Thermal stability of SFTs in Cu. Workshop on damage production, accumulation and consequences, Liverpool (GB), 6-7 Aug 2001. Unpublished.

Singh, B.N., Experiment, theoretical modelling and simulations. ITEM network kick-off meeting, Fontainebleau (FR), 22-23 Nov 2001. Unpublished.

Singh, B.N., Damage accumulation and materials response. ITEM network kick-off meeting, Fontainebleau (FR), 22-23 Nov 2001. Unpublished.

Singh, B.N.; Ghoniem, N.M.; Trinkaus, H., Experiment-based modeling of localized plasticity in irradiated metals. 10. International conference on fusion reactor materials (ICFRM 10), Baden-Baden (DE), 14-19 Oct 2001. Unpublished. Abstract available

Singh, B.N.; Toft, P.; Stubbins, J.F.; Tähtinen, S., Low cycle fatigue behaviour of unirradiated and neutron irradiated titanium alloys. 10. International conference on fusion reactor materials (ICFRM 10), Baden-Baden (DE), 14-19 Oct 2001. Unpublished. Abstract available

Singh, B.N.; Toft, P.; Stubbins, J.F.; Tähtinen, S., Creep-fatigue interaction and creep-crack growth behaviour of a dispersion hardened copper alloy before and after neutron irradiation. 10. International conference on fusion reactor materials (ICFRM 10), Baden-Baden (DE), 14-19 Oct 2001. Unpublished. Abstract available

Singh, B.N.; Zinkle, S.J., Role of microstructure in plastic flow localization. 2001 MRS Spring meeting. Symposium BB: Material instabilities and patterning in metals, San Francisco, CA (US), 17-18 Apr 2001. Unpublished.

Trinkaus, H.; Singh, B.N., Modeling void nucleation under cascade damage conditions. 10. International conference on fusion reactor materials (ICFRM 10), Baden-Baden (DE), 14-19 Oct 2001. Unpublished. Abstract available

Tähtinen, S.; Laukkanen, A.; Singh, B.N., Properties of copper to stainless steel hip - joints before and after neutron irradiation. 10. International conference on fusion reactor materials (ICFRM 10), Baden-Baden (DE), 14-19 Oct 2001. Unpublished. Abstract available

Tähtinen, S.; Moilanen, P.; Singh, B.N., Tensile and fracture toughness properties of neutron irradiated titanium alloys. 10. International conference on fusion reactor materials (ICFRM 10), Baden-Baden (DE), 14-19 Oct 2001. Unpublished. Abstract available

Zinkle, S.J.; Singh, B.N:; Hashimoto, N.; Hoelzer, D.T., Effect of periodic temperature variations on the microstructure of neutron-irradiated metals. 10. International conference on fusion reactor materials (ICFRM 10), Baden-Baden (DE), 14-19 Oct 2001. Unpublished. Abstract available.

Title and authors

Association Euratom – Risø National Laboratory
Annual Progress Report 2001

Edited by H. Bindslev and B.N. Singh

ISBN	ISSN
87-550-3064-5 87-550-3065-3 (Internet)	0106-2840; 1396-3449

Department or group	Date
Optics and Fluid Dynamics Department	June 2002

Pages	Tables	Illustrations	References
49		31	15

Abstract (max. 2000 characters)

The programme of the Research Unit of the Fusion Association Euratom - Risø National Laboratory covers work in fusion plasma physics and in fusion technology. The fusion plasma physics research focuses on turbulence and transport, and its interaction with the plasma equilibrium and particles. The effort includes both first principles based modelling, and experimental observations of turbulence and of fast ion dynamics by collective Thomson scattering. The activities in technology cover investigations of radiation damage of fusion reactor materials. These activities contribute to the Next Step, the Long-term and the Underlying Fusion Technology programme. A summary is presented of the results obtained in the Research Unit during 2001.

Descriptors INIS/EDB

LASER DOPPLER ANEMOMETERS; MAGNETIC CONFINEMENT; NONLINEAR PROBLEMS; NUMERICAL SOLUTION; PELLET INJECTION; PHYSICAL RADIATION EFFECTS; PLASMA DIAGNOSTICS; PLASMA SCRAPE-OFF LAYER; PLASMA SIMULATION; PROGRESS REPORT; RISOE NATIONAL LABORATORY; THERMONUCLEAR REACTOR MATERIALS; TOKAMAK DEVICES; TURBULENCE; VORTICES

Available on request from Information Service Department, Risø National Laboratory,
(Afdelingen for Informationsservice, Forskningscenter Risø), P.O.Box 49, DK-4000 Roskilde, Denmark.
Telephone +45 4677 4004, Telefax +45 4677 4013, email: risoe@risoe.dk